TKK Dissertations 4
Espoo 2005

PERFORMANCE AND MODELING OF MAGNETIC SHAPE MEMORY ACTUATORS AND SENSORS

Doctoral Dissertation

Ilkka Suorsa

Helsinki University of Technology
Department of Electrical and Communications Engineering
Laboratory of Electromechanics

TKK Dissertations 4
Espoo 2005

PERFORMANCE AND MODELING OF MAGNETIC SHAPE MEMORY ACTUATORS AND SENSORS

Doctoral Dissertation

Ilkka Suorsa

Dissertation for the degree of Doctor of Science in Technology to be presented with due permission of the Department of Electrical and Communications Engineering for public examination and debate in Auditorium S4 at Helsinki University of Technology (Espoo, Finland) on the 16th of May, 2005, at 12 o'clock noon.

Helsinki University of Technology
Department of Electrical and Communications Engineering
Laboratory of Electromechanics

Teknillinen korkeakoulu
Sähkö- ja tietoliikennetekniikan osasto
Sähkömekaniikan laboratorio

Distribution:
Helsinki University of Technology
Department of Electrical and Communications Engineering
Laboratory of Electromechanics
P.O.Box 3000
FI - 02015 TKK
URL: http://www.sahko.tkk.fi/
Tel. + 358 9 451 2384
Fax. + 358 9 451 2991
E-mail: Ilkka.Suorsa@tkk.fi

ISBN 951-22-7644-5
ISBN 951-22-7645-3 (PDF)
ISSN 1795-2239
ISSN 1795-4584 (PDF)
URL: http://lib.tkk.fi/Diss/2005/isbn9512276453/

TKK-DISS-1987

Otamedia Oy
Espoo 2005

HELSINKI UNIVERSITY OF TECHNOLOGY
P.O. BOX 1000, FIN-02015 HUT
http://www.hut.fi

ABSTRACT OF DOCTORAL DISSERTATION

Author Ilkka Suorsa

Name of the dissertation

Performance and modeling of magnetic shape memory actuators and sensors

Date of manuscript

Date of the dissertation 16.5.2005

☐ Monograph

☑ Article dissertation (summary + original articles)

Department Electrical and Communication Engineering

Laboratory Electromechanics

Field of research Electromechanics

Opponent(s) Professor Manfred Wuttig, University of Maryland, USA

Supervisor Professor Antero Arkkio

(Instructor) Dr. Juhani Tellinen

Abstract

Magnetic Shape Memory (MSM) materials comprise a new active material type, which can change its shape in magnetic fields. Non-stoichiometric Ni-Mn-Ga in 5M martensite is the most utilized MSM material so far. It has been used also in this study. The material has also a reverse effect: the change in shape of the material with non-zero magnetization alters the magnetic field in which it is placed. Due to its properties, the material has two promising applications: motion-generating actuators and sensors. In this work, both sensors and actuators are studied with interest focused on the modeling and operation parameters of the applications. A lumped parameter model for contruction of an actuator and a sensor consisting of models for MSM effect and magnetic, mechanical and electric circuits of the application has been made. The models have been tested with measurements.

In addition, the properties of the material itself have been studied. The magnetic field induced stress and the magnetization dependence on strain have been measured. The magnetic field induced stress in MSM material was found to be in accordance with existing theory. Under high magnetic fields, the measured magnetization dependence on strain was also predicted by the existing theory. However, a new functional dependence was found under low magnetic fields. New MSM applications have been built and tested as linear motors and speed sensors. The speed sensor can also be used as a voltage generator. Associated with the linear motor, a control system for MSM actuators was studied and built.

Keywords Magnetic shape memory material, Ni-Mn-Ga, sensors, actuators, magnetic modeling

Number of pages 70 p. + app. 28 p.

ISBN (printed) 951-22-7644-5

ISBN (pdf) 951-22-7645-3

ISBN (others)

ISSN (printed) 1795-2239

ISSN (pdf) 1795-4584

Publisher Helsinki University of Technology, Laboratory of Electromechanics

Print distribution Helsinki University of Technology, Laboratory of Electromechanics

☑ The dissertation can be read at http://lib.hut.fi/Diss/ 2005/isbn9512276453

Preface

This work began in Laboratory of Electromechanics in Helsinki University of Technology (HUT), where the topic concerning the Magnetic Shape Memory (MSM) material was introduced to me by Professor Tapani Jokinen. Later when I was working in Adaptamat Ltd, Professor Antero Arkkio helped me to finish my thesis. I thank them both for assistance. During my study, I have also been in contact with other research people studying MSM materials in HUT. I am grateful to them for fruitful discussions about the MSM material properties.

The main work of this thesis was done in the Adaptamat Ltd., where my colleagues assisted my work. I thank Kari Ullakko, Emmanouel Pagounis and Ilkka Aaltio, who participated in writing the articles included in this thesis. Olli Mattila I thank for making the MSM elements for the study. Most importantly I thank my instructor Juhani Tellinen, who gave valuable comments and instructions during this thesis work. He also participated in doing the articles included in the thesis.

I am grateful for the Foundation of Technology in Finland - TES and the Finnish Foundation for Economic and Technology Sciences - KAUTE and Adaptamat Ltd. for the financial support.

Finally I thank my wife Ying for the encouragement and comments during the research work.

Helsinki, November 2004

Ilkka Suorsa

Publications

[P1] Suorsa I. and Pagounis E., "Magnetic field-induced stress in the Ni-Mn-Ga magnetic shape memory alloy", Journal of Applied Physics, Vol. 95 (2004) No. 10, pp. 4958-4961.

[P2] Suorsa I., Pagounis E. and Ullakko K., "Magnetization dependence on strain in the Ni-Mn-Ga magnetic shape memory material", Applied Physics Letters, Vol. 84 (2004) No. 23, pp. 4658-4660.

[P3] Suorsa I., Tellinen J., Ullakko K. and Pagounis E., "Voltage generation induced by mechanical straining in magnetic shape memory materials", Journal of Applied Physics, Vol. 95 (2004) No. 11, pp. 8054-8058.

[P4] Suorsa I., Pagounis E. and Ullakko K., "Magnetic shape memory actuator performance", Journal of Magnetism and Magnetic Materials, Vol. 272-276 (2003), pp. 2029-2030.

[P5] Suorsa I., Tellinen J., Pagounis E., Aaltio I. and Ullakko K., "Applications of Magnetic Shape Memory Actuators", Proc. of Actuator 2002 conference, 12-14 June 2002, Bremen, Germany, pp. 158-161.

[P6] Suorsa I., Tellinen J., Aaltio I., Pagounis E. and Ullakko K., "Design of Active Element for MSM Actuator", Proc. of Actuator 2004 Conference, 14-16 June 2004, Bremen, Germany, pp. 573-576.

Contents

List of symbols

A_{cross}	cross-section area
A_{side}	side area
a	lattice parameter
B	magnetic flux density
B_a	magnetic flux density in easy magnetization direction (axial direction)
B_i	intrinsic induction
B_{is}	saturation intrinsic induction
B_{MSM}	effective flux density in MSM material
B_t	magnetic flux density in hard magnetization direction (transverse direction)
C	effective stiffness
c	lattice parameter
E_k	magnetization energy density
F	force
F_{ext}	external force
F_{mag}	magnetic field induced force
F_{spring}	spring force
f	driving force
f_1	first variant volume fraction
f_2	second variant volume fraction
i	current
H	magnetic field strength
H_{MSM}	effective magnetic field strength in the MSM material
H_s	saturation magnetic field strength
H_{sw}	switching magnetic field strength
K_1	crystal anisotropy constant
K_2	crystal anisotropy constant
K_3	crystal anisotropy constant
l	length
M	magnetization

M_a	magnetization in easy magnetization direction (axial direction)
M_i	magnetization of a variant
M_t	magnetization in hard magnetization direction (transverse direction)
M_s	saturation magnetization
m	mass
m_{eff}	relative magnetization
N	number of turns
q	loss density
R_m	reluctance
R_{m1}	reluctance
R_{mC}	reluctance of the core of the actuator
R_{mG}	reluctance of the air-gap
T_{as}	Austenite start temperature
T_c	Curie temperature
T_M	martensite transformation temperature
U_m	magnetomotive force (magnetic voltage)
$U_{m,coil}$	coil magnetomotive force
u_e	electric voltage
w	width of the element
w_a	anisotropy energy density
w_{int}	internal energy density
w_m	magnetization energy density
w_{mag}	magnetic energy density
w_{mech}	mechanical energy density
w_z	Zeeman energy density
$\boldsymbol{u}_x$	unit vector to the direction of the x axis
$\boldsymbol{u}_y$	unit vector to the direction of the y axis
x	volume fraction of a variant
α	angle between the lattice axis and the external magnetic field
α_p	volume fraction of the domains
β	angle between the lattice axis and the external magnetic field

χ	susceptibility
Δl	change in length
δ	geometrical angle
ε	strain
ε_0	crystallographic limit strain
ε_{max}	maximum measured strain
Φ	magnetic flux
Φ_{PM}	magnetic flux of the permanent magnets
ϕ	angle between the lattice axis and the external magnetic field
γ	surface angle of the variant boundary in the MSM element
μ	permeability
μ_a	permeability of the easy magnetization direction (axial direction)
μ_t	permeability of the hard magnetization direction (transverse direction)
μ_0	permeability of the vacuum
ψ	surface angle of the variant boundary in the MSM element
σ	stress
σ_{mag}	magnetic field induced stress
σ_{mech}	mechanical stress
σ_{TW}	twinning stress
$\sigma_{TW,ave}$	average twinning stress
θ	angle between the magnetization vector and the external magnetic field
θ_i	angle between the magnetization vector and the external magnetic field in a variant
ζ	geometrical angle

Abbreviations

AC	Alternating current
DC	Direct current
CLS	Crystallographic limit strain
ED	Easy magnetization direction
FSM	Ferromagnetic shape memory
HD	Hard magnetization direction
MFI	Magnetic field induced
MSM	Magnetic shape memory
PM	Permanent magnet
VSM	Vibrating sample magnetometer
5M	5 layered martensite
7M	7 layered martensite

1 INTRODUCTION

One central part of electromechanics is how to generate mechanical energy from electrical energy. There are many different ways of doing this. Traditionally, the most used devices for such energy transformation are the electrical machines that use magnetic fields for the energy conversion. More and more commonly, so called active materials are utilized for the motion generation. These materials have special properties that allow their shape to be changed in different fields, like electric or magnetic fields, or under a change of temperature. They are especially useful when the amount of the transferred energy is small. So far, at higher energy levels the traditional electrical machines are more economic and efficient than the active materials.

In this work, an active material called the Magnetic Shape Memory (MSM) [72] or Ferromagnetic Shape Memory (FSM) [5] material has been studied. The MSM materials are a recently discovered new group of materials [72,74] that can change their shape in a magnetic field. As in the case of all active materials, this material type also has a reverse effect, i.e. changes in the shape of the materials with non-zero magnetization influence the magnetic fields they are in. Due to the motion generation and the reverse effect, the two most promising applications of the material are actuators and sensors. Both of these have been studied in this work.

Economically, the most successful active materials so far are the piezo electric materials, which can change their shape in an electrical field. The shape change in these materials is small, but the induced stress is large and the associated actuator construction compact. In addition, with intelligent technical constructions it is possible to multiply the small stroke of the piezo element, see e.g. [71]. There are also other electric field operated active materials such as the electroactive polymers (see e.g. [35]) and electro-rheological fluids, see e.g. [4]. Another commonly used active material group is composed of the giant magnetostrictive materials, which change their shape in magnetic fields. Magnetostriction can be described as a deformation of a body in response to a change in magnetization of the material [8]; it occurs in many different materials. The giant magnetostrictive materials have a particularly high magnetostriction strain and are therefore used as active materials. Due to the same triggering field and definition of the

magnetostriction, the MSM effect is sometimes called magnetostriction [18] or twin-induced magnetostriction [53]. However, the MSM effect is different from the phenomenon that causes the classic magnetostriction, so, in this work, these two are considered different concepts. Important difference between the classic magnetostriction and MSM effect is the magnitude of strain. Magnetostriction strain is much smaller than MSM strain.

Shape memory materials generate a shape change due to the phase transformation in the material from austenite to martensite, see e.g. [11]. The shape change in shape memory materials is large but due to the phase transformation, the motion is slow. The shape memory effect can also be observed in MSM materials when the material is heated above the martensite-austenite transformation temperature [5]. The MSM effect itself occurs in the martensite phase and does not need a phase transformation. This makes the magnetic field triggered MSM effect considerably faster than the ordinary shape memory effect.

Active materials have many different properties that define their usability for different applications. Relative shape change or strain is one of the key parameters of an active material. Shape change in MSM material is huge, up to 10%- strains have been measured from MSM material [57]. This is considerably more than in an average piezoceramic or magnetostrictive material. This fact has triggered a lot of interest in MSM material study. However, the amount of generated strain is not the only important parameter for active material. Output stress, for example, and controllability, speed of change and the needed external components for material operation are also essential considerations when determining the benefits of different materials.

1.1 Aim of the work

Only a limited number of MSM applications or their models have been studied prior to this work. The aim of this work was to examine the most promising applications of the MSM material, sensors and actuators. The main interest is focused on the operation parameters and the models of those applications and the MSM material itself.

1.2 Scientific contributions of the work

The scientific contribution of this work can be summarized as

- The Magnetic Field Induced (MFI) stress is an essential parameter of the MSM material. In this work, the stress generated by the material was measured as being in accordance with the previously introduced model.
- The magnetization of the material was measured as a function of the strain in the material. For sensor applications, the magnetization dependence on strain is crucial. A new dependence was found at low magnetic field strength values. This result is important, because the sensor applications are best operated at this range.
- Several actuator properties were studied: fatigue life, positioning accuracy, rise-time, acceleration and speed.
- A new motion generation application, an MSM linear motor, was built. The properties of the motor, positioning accuracy and speed, were recorded.
- The control of the MSM applications has been studied and a control system for MSM actuators and linear motors has been built. Only very limited studies of the control of MSM actuators have been conducted prior to this work.
- A new MSM sensor application, a velocity sensor, was built and tested. It demonstrated a very large voltage generation capability. The sensor was modeled and the results were compared with measurements.
- MSM actuator models, including an existing MSM material model, were built. The actuator model includes the magnetic circuit models for the MSM actuator, which have not been published prior to this work. The measured results from an MSM actuator were compared with the calculated ones.

1.3 Structure of the work

This thesis consists of a review of the basic physics related to the magnetic fields (Chapter 2), properties of the MSM material (Chapter 3), models of the MSM material

(Chapter 4) and the applications, actuators (Chapter 5) and sensors (Chapter 6). The discussion in Chapter 7 clarifies the scientific contribution of the present thesis. Six publications, as part of this work, are included at the end of the thesis. The content of the articles is as follows.

Publication P1

The publication describes a method of measuring the magnetic field induced stress in MSM material. The article also describes a previously developed model of MFI stress and compares the measured and calculated results. The accuracy of the model is found to be good. This is crucial for the use of the MSM material model, both separately as well as a part of the actuator models.

Ilkka Suorsa made the measurements and the calculation related to the model. The article was written by Ilkka Suorsa and Emmanouel Pagounis. In addition Juhani Tellinen as well as Aleksei Sozinov is acknowledged for their comments about the text.

Publication P2

The magnetization of the MSM material depends on its strain state. The material model needs this dependence, which directly defines the sensor application outputs, especially when the material is used as a position sensor. In this article, the strain dependence is measured and the measurement set-up is designed and described. A new dependence is found at lower magnetic field strength values, which is crucial in understanding the MSM sensor outputs. A new theoretical reason for the new dependence is proposed.

Ilkka Suorsa performed the measurements and formulated the models of the magnetization. The text was written by Ilkka Suorsa and Emmanouel Pagounis. Kari Ullakko gave valuable comments about the text.

Publication P3

When MSM material is in a magnetic field and its shape is changed, it consequently alters the magnetic field. This in turn can be used to produce voltage. This article shows for the first time that MSM material can be used as a voltage generator to produce large

voltages. In addition, the article demonstrates that an MSM actuator can be used as a speed sensor. The theoretical dependence between the speed and induced voltage is shown. A model to solve the instantaneous values of the induced voltage is proposed. The modeled results are compared with the measurements. A sufficiently good agreement between the measured and the calculated values is found. The model for the permanent magnet MSM actuator magnetic circuit is presented for the first time.

The measurements and the modeling for magnetization dependence on strain were performed by Ilkka Suorsa. The co-authors to this article were Juhani Tellinen, Emmanouel Pagounis and Kari Ullakko. The article was written by Ilkka Suorsa and Emmanouel Pagounis. Juhani Tellinen built the original magnetic circuit model for the MSM actuator, which was altered by Ilkka Suorsa. The original idea for the measurements was initiated by Kari Ullakko, who gave valuable comments about the article.

Publication P4

This article presents measured quantities of dynamic behavior of an MSM, namely the speed and the acceleration it is possible to generate with an MSM actuator. Other properties of the MSM actuators are discussed, too.

The text was written and the measurements were obtained by Ilkka Suorsa. The co-authors of this article, Emmanouel Pagounis and Kari Ullakko, gave valuable comments about the text.

Publication P5

This article is about MSM actuator applications. Three example applications are presented: MSM pump, MSM proportional valve and MSM linear motor. Measured results from the devices are explained. The driving circuit of the MSM actuator and linear motor is also discussed and demonstrated. The positioning accuracy and the speed of the linear motor were examined and found very good.

The text was written by Ilkka Suorsa, who also designed and tested the linear motor and the control system. The co-authors of this article are Juhani Tellinen, Ilkka Aaltio, Emmanouel Pagounis and Kari Ullakko, who participated in writing the article. In

addition, Juhani Tellinen designed and tested the valve and pump applications of the article.

Publication P6

This article presents a method of designing an MSM actuator. The main part of the article consists of an actuator model. The magnetic circuit model for an MSM actuator without permanent magnets is presented for the first time. The sub-models for the magnetic field induced stress, the twinning stress hysteresis, and the mechanical circuit are included.

The text was written by Ilkka Suorsa, who also made the measurements as well the model for the actuator and the calculations. Juhani Tellinen made the design equations for the MSM element and Emmanouel Pagounis assisted in writing the article. In addition, co-authors Juhani Tellinen, Ilkka Aaltio, Emmanouel Pagounis and Kari Ullakko gave valuable comments for the text.

2 MAGNETIC FIELDS

A central property of MSM material is its ability to generate stress in a magnetic field. For the modeling of the material it is important to model the magnetic fields. These are defined by the well-known Maxwell's equations, see e.g. [46]. When materials are placed in a magnetic field they interact with the field. The interaction depends strongly on the properties of the materials; they are divided into different groups basing on their response. MSM material is a ferromagnetic material, which reacts strongly with the field. When a piece of the material is placed in magnetic field H, it increases the magnetic flux density B caused by the field with the material's own magnetization M, see e.g. [46],

$$B=\mu_0(H+M) \quad , \tag{2.1}$$

where μ_0 is the permeability of the vacuum. The flux density caused by the magnetization of the material is called the intrinsic induction B_i

$$B_i=\mu_0 M=B-\mu_0 H \quad . \tag{2.2}$$

The magnetic properties of the material can also be determined with permeability μ or susceptibility χ, which are defined as

$$\mu=\frac{B}{H} \quad , \tag{2.3}$$

$$\chi=\frac{M}{H} \quad . \tag{2.4}$$

Due to their definitions, these parameters are connected to each other, $\mu/\mu_0 = 1+\chi$. In a linear magnetic material, susceptibility and permeability are constant. In ferromagnetic materials, the H - M relationship can be assumed linear only in some range of magnetic field values. Generally, they are nonlinear. The magnetization M depends on the magnetic field strength, which can be defined with a curve (see Fig. 1). The materials

have a saturation magnetization M_S, which is the maximum magnetization. It is achieved at a saturation field strength H_s. With higher magnetic field strength values, the material's magnetization does not increase.

2.1 Energies related to material in a magnetic field

There are many magnetic energy densities related to a ferromagnetic material in magnetic field. The energy density needed to generate the magnetization of the material is called the energy density of magnetization, w_m. When a material is moved to the magnetic field, the field causes a force on the element. Similarly, when the element is moved out of the magnetic field, an external force has to be used. The energy density caused by this force is called the internal energy density w_{int} (or the work done to the material or the co-energy), see e.g. [46]. This can also be seen as the potential energy that the material has in the magnetic field. The two energy densities can be derived as [3]

$$w_m = \int_0^{B_i} H dB_i = \mu_0 \int_0^M H dM \,, \tag{2.5}$$

$$w_{int} = -\int_0^H B_i dH = -\mu_0 \int_0^H M dH \,. \tag{2.6}$$

The internal energy density is negative, because the magnetic field pulls the material towards itself and causes negative external force. Since the energies are in integral form they can be represented with areas related to the magnetization curve of the material (see Fig. 1).

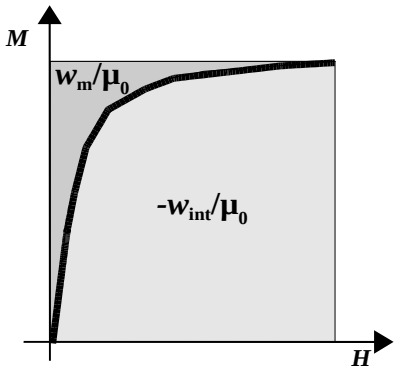

Fig. 1. Magnetization curve and the areas representing the magnetic field related energies in a ferromagnetic material.

If the external force is needed due to the rotation of a constant magnetization vector of the material, the related energy can be called the Zeeman energy density w_z. It represents the potential energy in the rotation of the magnetization vector $\boldsymbol{M}_s$ in an applied field $\boldsymbol{H}$ [46]

$$w_z = -\mu_0 \mathbf{M}_s \cdot \mathbf{H} = -\mu_0 M_s H \cos\theta \ , \qquad (2.7)$$

where θ is the angle between the magnetization vector M_s and the external magnetic field H.

2.2 Magnetic anisotropy

A material is called magnetically anisotropic if the magnetization curve of the material depends on the direction to which the material is magnetized. Some directions need only a little energy to be magnetized, while others need more. The direction that is easy to magnetize is called the easy magnetization direction (ED). The direction that needs most energy to be magnetized is called the hard magnetization direction (HD). Fig. 2 presents schematic views of the magnetization curves in HD and ED in the MSM material.

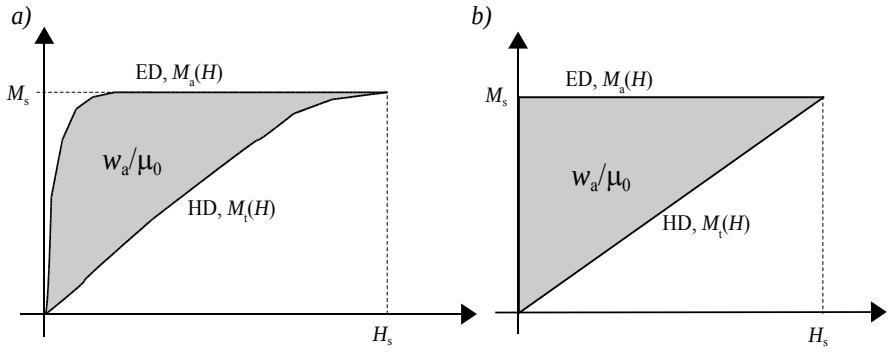

Fig. 2. a) Schematic view of easy and hard magnetization direction magnetization curves and b) simplified magnetization curves. The anisotropy energy density is proportional to the shaded areas in the figure.

It is convenient to model the energy of anisotropy with crystal anisotropy constants. The crystal anisotropy energy density E_k represents the energy density needed to magnetize the material to a saturation level, M_s, in a specific lattice direction. In the case where a single-crystal material has a tetragonal unit cell, the magnetization energy density of the crystal, E_k, can be expressed as [3]

$$E_k = K_0 + K_1 \sin^2\phi + K_2 \sin^4\phi + K_3 \cos^2\alpha \cos^2\beta \qquad (2.8)$$

where K_0, K_1, K_2 and K_3 are anisotropy constants, ϕ, α and β are the angles between the lattice directions and the external magnetic field. The anisotropy constants can be measured experimentally. The main interest is in the energy differences between two directions, so the constant term K_0 can be left out of considerations. In practice, in the case of 5-layered martensite Ni-Mn-Ga MSM material, it is usually sufficient to model the anisotropy with only one parameter K_1. In this case, Eq. (2.8) describes a uniaxial anisotropy, i.e. it has one easy magnetization direction and a plane of hard magnetization directions. This is not general for MSM materials. For example, MSM materials with the orthorhombic unit cell structure do not have uniaxial anisotropy.

The most interesting anisotropy energy density difference is the difference between the ED axis and HD plane, w_a. This anisotropy energy density is represented by the

shaded area in Fig 2. Since it is a closed area defined by monotonic functions, it can be calculated with two integrals

$$w_a = \mu_0 \int_0^{M_s} (H_a - H_t) dM = \mu_0 \int_0^{H_s} (M_a - M_t) dH , \qquad (2.9)$$

where H_a is the magnetic field strength in the ED (axial direction), H_t the magnetic field strength in the HD (transverse direction), H_s the saturation field strength, M_a the magnetization in the ED, M_t the magnetization in the HD and M_s the saturation magnetization. The MSM materials magnetization process in HD is a rotation of the magnetization vector, while in the ED the magnetization increases due to the domain wall movement. This result is common for the anisotropic materials [46]. Due to different magnetization processes, the measured ED curves have significant hysteresis, while HD magnetization curves do not [38,**P2**]. In a simplified case, the magnetization of the HD of a uniaxial material, like MSM material, can be modeled as $M = M_s \cos\theta$, where θ is the angle between the magnetization vector and the external magnetic field. As function of magnetic field strength, the HD magnetization curve becomes linear [46]. The magnetization through the domain wall movement is easier. In the simplified case, one can assume the initial permeability of the MSM material to be infinite. The schematic view of the corresponding simplified magnetization curves in HD and ED as a function of the magnetic field strength is shown in Fig. 2b. With these assumptions, the magnetization energy w_m in the HD as a function of the magnetization rotation angle θ can be written as

$$w_m = K_1 \cos^2\theta . \qquad (2.10)$$

2.3 Magnetic circuits

Both magnetic and electric systems can be modeled with circuit equations. The magnetic flux Φ and magnetomotive force U_m (or magnetic voltage) of the magnetic circuit behave similarly as the electric current i and voltage u_e of the electric circuit. The magnetic voltage can be expressed as a function of field strength $U_m = H\,l$. Similarly, the flux can be expressed as function of flux density $\Phi = B\,A$. The reluctance of a magnetic circuit is equivalent to the resistance of an electric circuit. The reluctance R_m of a homogeneous piece of material with permeability μ, cross-section A, and length l is

$$R_m = \frac{U_m}{\Phi} = \frac{1}{\mu}\frac{l}{A} \ . \qquad (2.11)$$

The magnetic field can be generated with permanent magnets or current conducting coils. The magnetomotive force $U_{m,coil}$ generated by a coil with N turns and current i is $U_{m,coil} = N\,i$. The modeling of a permanent magnet can be more complicated than that of a simple coil. In this work, a constant flux source Φ_{PM} was used to represent the permanent magnet (see Fig 3). This model is valid if the permanent magnet flux is independent of the changes in the magnetic circuit. It is a good approximation in MSM actuators that have been built so far.

A whole magnetic system consisting of coils, permanent magnets and a ferromagnetic core can now be represented with a reluctance network model. This system is called a magnetic circuit. A magnetic circuit model of an MSM actuator can be seen in Fig. 3. The resulting lumped parameter model is simple and the field strength and flux density in different parts of the actuator can be calculated.

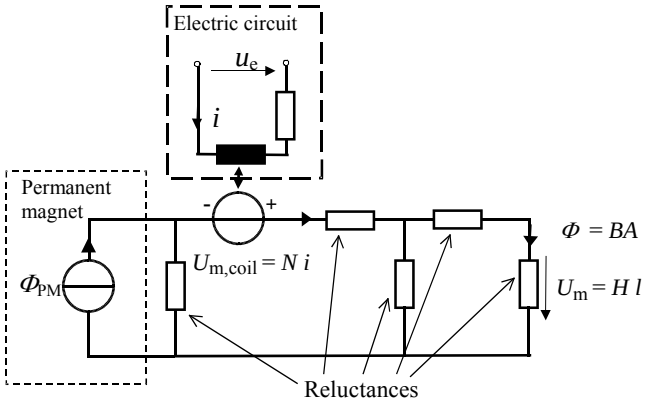

Fig. 3. Magnetic circuit model for an MSM actuator with permanent magnets

3 MSM MATERIALS

The materials showing MSM effects have a non-cubic unit cell structure. The shape change effect itself is based on the reorientation of the unit cells in the material. Since the unit cells are not symmetric, the deformation results in a change of the macroscopic shape of the material. A special property of MSM material is that the energy needed for deforming the unit cells is small, much smaller than in most materials. In addition, MSM materials have strong magnetic anisotropy, because the anisotropic unit cells can be reoriented with the magnetic field. Another way of generating the shape change is to apply a mechanical stress on the material in an elongated direction.

The highest MFI strain has been measured from a single crystal Ni-Mn-Ga material, up to 10% have been recorded [57]. Polycrystalline Ni-Mn-Ga also shows some MFI strain [73,50,9] but it is not as high as in single crystals. There are also other materials showing the MSM effect, FePd [18], FePt [23], NiGaFe [47] and CoNiGa [75]. In the case of Fe_3Pd several percents of reversible MFI strain have been demonstrated [56,54]. Composition CoNiAl has shown recoverable stress- induced strain of up to 4 % [24]. However, in this case the required mechanical stress is considerably higher and cannot be produced with a magnetic field.

3.1 Ni-Mn-Ga MSM material

Metals exhibit different phases in the solid state. As the different phases have a different susceptibility, the phase transformations can be seen as changes in the susceptibility. In the case of Fig. 4, a tested Ni-Mn-Ga material was first heated and then cooled down. The cooling curve is visible in the Fig. 4. When the temperature drops, the material first comes to Curie temperature, at which it turns ferromagnetic. The material is now in the austenite phase. When it is cooled further, there is another large change in susceptibility, which indicates the material is changing into martensite. The exact austenite martensite transformation temperature depends on the composition of the material. In addition, the mechanical stress and the magnetic field in the material affect this temperature [19,6]. In Ni-Mn-Ga, the MSM effect occurs in the martensite phase. Different types of martensite

can be formed in the material. From the point of view of MSM effect, the two most important martensite phases found from Ni-Mn-Ga are the 7-layered (7M) and 5-layered (5M) martensites. The 5M martensite has a tetragonal unit cell structure while the 7M martensite has an orthorhombic one [52,37]. The lattice structure is deformed in a cyclic way in periods of 5 or 7 atomic layers, which explains the naming of these martensites [52]. The martensite type in an MSM material depends on its composition as well as the temperature. The lattice parameters have been measured in specific compositions and different martensites [59]. An important property that can be calculated with the lattice parameters is the Crystallographic Limit Strain (CLS) $\varepsilon_0 = 1\text{-}c/a$. It is the maximum strain that the material can generate by reorienting unit cells. In 5M martensite, the CLS is 5.9 %, and in 7M martensite, it is 10.7 % [59]. Since the unit cell parameters are temperature dependent, the CLS is too. The CLS ε_0 is the upper bound of the maximum measured strain from a material element ε_{max}, i.e. $\varepsilon_{max} \leq \varepsilon_0$.

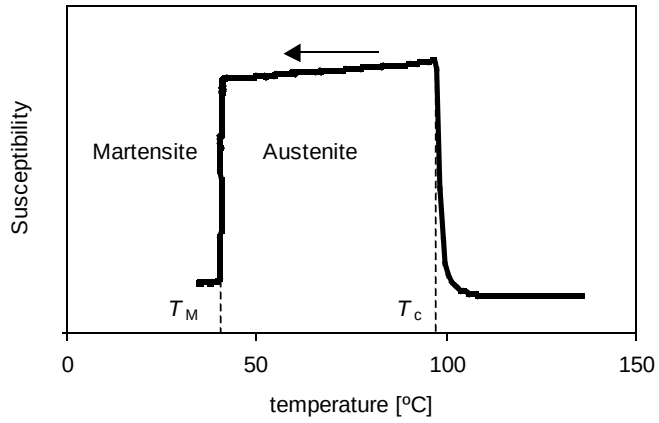

Fig. 4. Typical susceptibility measurement result from Ni-Mn-Ga alloy. The susceptibility was measured, when the temperature was dropping. The austenite-martensite transformation temperature T_M and Curie temperature T_C are marked in the figure. The transition temperatures vary depending on the composition and manufacturing of the material.

The tetragonal 5M Ni-Mn-Ga in a martensite phase is so far the most promising MSM application material. It gives about 6% strain and has a maximum MFI stress close to 3 MPa. The highest shape changes have been reported from 7M martensite orthorhombic structure, which has a composition of $Ni_{48.8}Mn_{29.7}Ga_{21.5}$ [57]. This material has been measured to give an as high as 9.6 % MFI strain. The mechanically induced deformation is even higher, close to 11%. The strains are indicated by the lattice CLS of the material. Similar results from 7-layered martensite have also been reported from an alloy with a composition of $Ni_{50.0}Mn_{29.4}Ga_{20.6}$ [42]. Even though the lattice distortion increases the magnetic anisotropy in Ni-Mn-Ga materials, the increase reduces with high lattice distortion values [59]. This reduces the MFI stress, which the high strain material can generate and is one reason why the 7M martensite is not used for applications. Another reason can be the more limiting temperature range of the 7M than 5M martensite. In addition, the 7M material needs a higher magnetic field for saturation [59].

The third interesting martensite phase measured in Ni-Mn-Ga is the non layered one, which has 20% CLS. This indicates a possibility of having MSM material with a huge 20% strain. However, the actual MFI strain measured from the material has been less than 0.02 % [57].

In this study, only single-crystal 5M MSM materials have been used. The composition has varied, but in all cases it has been close to (wt%) Ni49-Mn26-Ga25.

The strain-magnetic field relationship of the 5M martensite Ni-Mn-Ga material has been measured and reported in many publications, for example [29,21]. The strain forms a butterfly curve as a function of field strength or flux density. Examples of curves measured under different opposing stresses can be seen in Fig. 5. This curve shape is dependent on the material composition and processing as well as the temperature. The strain also depends on the opposing stress of the material.

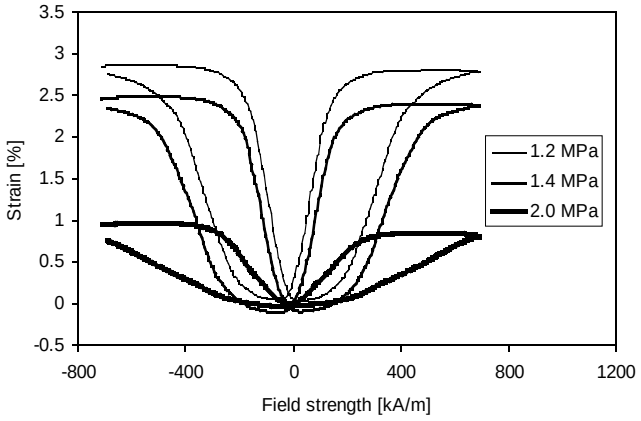

Fig. 5. Example measured strain-field curves of a single-crystal 5M Ni-Mn-Ga MSM material under different constant loads [21]. *The field has been measured outside the sample and it may have a significant error.*

3.1.1 Internal regions

Differently oriented unit cells form regions into the material, called the variant regions or twin variants. These are connected to each other with twin boundaries. When the MSM element size is changed we see these boundaries move, which is the result of unit cell deformation on the twin boundaries. An Ni-Mn-Ga MSM element made for axial deformation has twin boundaries in specific angles shown in Fig. 6. The composition of the element in Fig. 6 was (wt%) Ni49-Mn26-Ga25; it was 5M martensite with maximum strain $\varepsilon_{max} = 0.06$. It can be seen that the twin boundary angle on the other surface is close to 45º with respect to the element surfaces; on the other surface it is close to 90º.

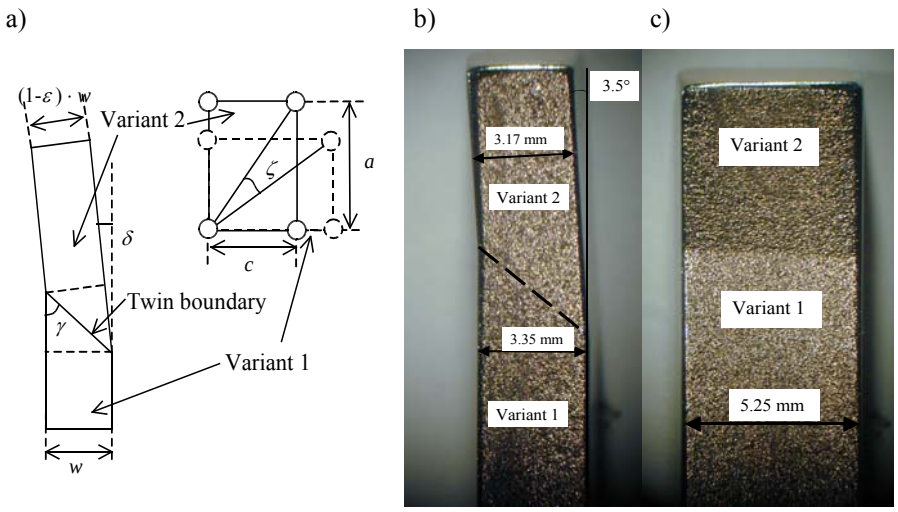

Fig. 6. a) A surface structure of a 5-layered MSM material element and the unit cell of the MSM material in the two variants. b) An optical photograph of the MSM element surface with one variant boundary. The variant boundary is not clearly visible on this surface since there is no tilt in this direction. The boundary is marked with a dashed line to the figure. c) Optical photograph of the other surface of the MSM element. On this surface, the variant boundary is clearly visible due to the mechanical tilt.

Since the two variants have differently oriented unit cells, the macroscopic width of the element, consisting of the two variants, is different as well. This results in tilting of the element from the twin boundary as can be seen in Figs. 6a and 6b. The tilting makes the twin boundary lines clearly visible on one surface of the MSM sample. The optical photos of an MSM element surfaces can be seen in Figs. 6b and 6c, when the material has one variant boundary. Based on the geometry of the element (see Fig. 6a) and the angle γ (= 49°), the tilting angle δ was calculated to be 3.5°. This same angle was also measured from the optical picture of the element (Fig. 6b). Interestingly, the same tilt angle could be found based on the unit cell distortion. With numerical testing, it seems that angle ζ in the unit cell is very close to the angle of the element δ (see Fig 6a). This has also been pointed out by Murray *et al*. [39]. The tilting of the element could be a problem for a linear motion MSM application. However, the overall tilt will be reduced at the ends of the element when the material consists of several variant boundaries.

Besides the variant distribution, another important material substructure is formed by the magnetic domains. Due to the anisotropy of the material, the variant areas and the magnetic domains are connected to each other. Typically, single-crystal materials with magnetic anisotropy have organized domain walls parallel to the ED. This is the case with the MSM material, too. Since the material consists of differently oriented variants, the domains form a substructure in each variant [48]. This has been demonstrated in MSM material surface optical pictures of an 5M martensite $Ni_{48}Mn_{30}Ga_{22}$ MSM sample [33]. A schematic view of substructures in the MSM element can be seen in Fig. 7. The domains in tetragonal martensite have been reported to have 180° domain walls as can be seen in Fig. 7 [14]. Paul *et al.* showed with a theoretical approach that the domain boundary on the variant edge is not always at the same point as the variant boundary [51]. This is the case especially when the material is under an external magnetic field. However, the difference predicted by the model is not large compared to the size of the variant in Fig 7. The material elements can consist of many variant systems. Generally the variant structure in an MSM material is dependent on the composition and the history of the MSM element. For example, a different internal area structure is formed in the 7M martensite [42].

Additionally, types of distributions of the internal areas different from Fig. 7 (5M martensite) have been observed. Müllner et al. have reported that 5M martensite $Ni_{51}Mn_{28}Ga_{21}$ material consists of macroscopic variant areas divided into domains, which in turn are subdivided into smaller internal twins [41]. Similarly, three different variant structures have been observed in $Ni_{49.5}Mn_{29.5}Ga_{21.5}$ in the martensite phase [37], one macroscopic variant system and two microscopic variant systems. These internal areas influence the magnetic field distribution and are important for the modeling of the material. In this work, however, only one variant system is considered in the modeling of the MSM element (see Fig. 7).

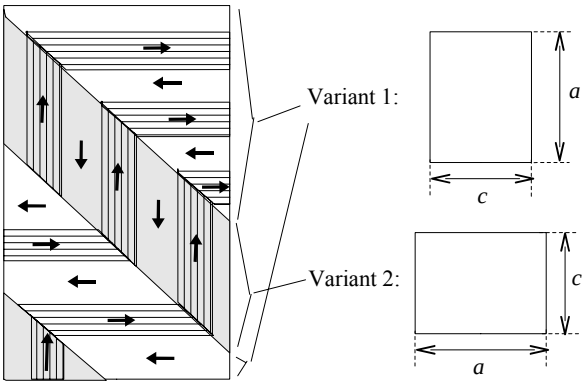

Fig 7. A schematic view of the assumed internal structure of the MSM element (see e.g. [17]). The directions of the magnetization of the domains are marked with arrows. The unit cell orientation in the variants is also visible in the figure.

3.1.2 Stress-strain relationship

When a material is placed under load, it is said to be in a state of stress. The uniaxial tensile stress σ of the material is defined as $\sigma = F/A$, where F is the tensile load acting perpendicularly to the surface and A is the surface area. Usually, the stress is defined as positive when it is elongating the material element. Under an elongating force, the material grows in length. The nominal strain is defined as $\varepsilon = \Delta l/l_0$ where Δl is the change in length of the element and l_0 the length of the element at zero strain. When the material is elongating in one direction, it contracts in the other direction(s). In the MSM material, a shape change is caused by rotation of unit cells, while the volume of an MSM element remains constant. In today's MSM material applications, the mechanical motion occurs in two orthogonal directions. The element consists of two variants; the ED of these variants is parallel to the directions of the mechanical motion. If the material is elongated in one direction, the elongation strain in this direction is very close to the value of contraction strain in the other moving direction. Since only two directions of the material are responding to the external stress and magnetic field, the length of the third direction remains constant. The non-moving direction is called the dead direction. Usually, the MSM elements are cut so that the surfaces of the rectangular element correspond to these

three directions, two moving and one dead direction. For applications it is sufficient to study the stress-strain relationship of the material just in the two moving directions. In addition, it is assumed that these directions are symmetric, so that the stress-strain curves in both directions are the same. With such assumptions the stress strain behavior of MSM material can be defined with only one curve. The characteristics of this curve depend on the composition and history of the element and the temperature [12]. Commonly, metals at low strains are elastic, i.e. the strain is linearly dependent on the applied stress. In MSM materials, this approximation is valid in the austenite phase. However, close to the martensite transformation temperature, it is possible to cause stress induced martensite to austenite, which will alter the linear stress-strain curve of the material [6].

To model the MSM effect, the stress-strain behavior of the material in the martensite has to be known. If the element is first elongated and then placed under uniaxial stress, it initially gives only little strain, but after a certain stress value, the strain grows rapidly. The large straining is due to the rotation of the unit cells in the material. Once all the unit cells have reoriented favorable to the external stress, the material becomes elastic and harder. Since the strain is caused by the unit cell reorientation, the maximum strain ε_{max} is equal to CLS, $\varepsilon_{max} = \varepsilon_0$. A measured stress-strain behavior of a 5M Ni-Mn-Ga MSM material can be seen in Fig. 8, which includes boundary curves ε_+ and ε_- as well as a few different size minor loop curves. Similar boundary curves have been measured earlier for 5M martensite [29] and for 7-layered martensite [57]. The needed initial stress can be seen as hysteresis in the stress-strain curve and it is called twinning stress. For characterization of the 5M Ni-Mn-Ga material, the parameter average twinning stress $\sigma_{TW,ave}$ is defined as the stress value of the boundary stress curve at 3% strain [12] (see Fig. 8). So far, this parameter has been measured to be $\sigma_{TW,ave} > 0.5$ MPa, depending on the composition and processing of the material. Because the mechanical hysteresis is the biggest cause of losses in the material, the average twinning stress is an important parameter. Due to the hysteresis, the MSM material can also be used as a damper. The mechanisms primarily responsible for the hysteresis have not yet been identified in detail. The hysteresis is probably affected by the defects and impurities in the MSM material. In microscopic modeling of the material, the localized defects have been used to model the twinning stress [51].

The response of material to the external or MFI stress has been modeled in different ways. Regardless of the nonlinearities, the simplest way is to assume a linear material stress-strain behavior [45,30]. As can be seen from Fig. 8, this is a rough approximation. For more accurate results, the minor stress-strain hysteresis loops have to be modeled [33,29,**P6**]. The hysteresis between the twinning stress and strain is similar to the magnetic one between the field strength *H* and the flux density *B*. In this work, a hysteresis model originally developed for magnetic hysteresis was used for modeling the mechanical hysteresis [65]. The calculated results for large hysteresis loops were in sufficient accordance with the measured results [**P6**].

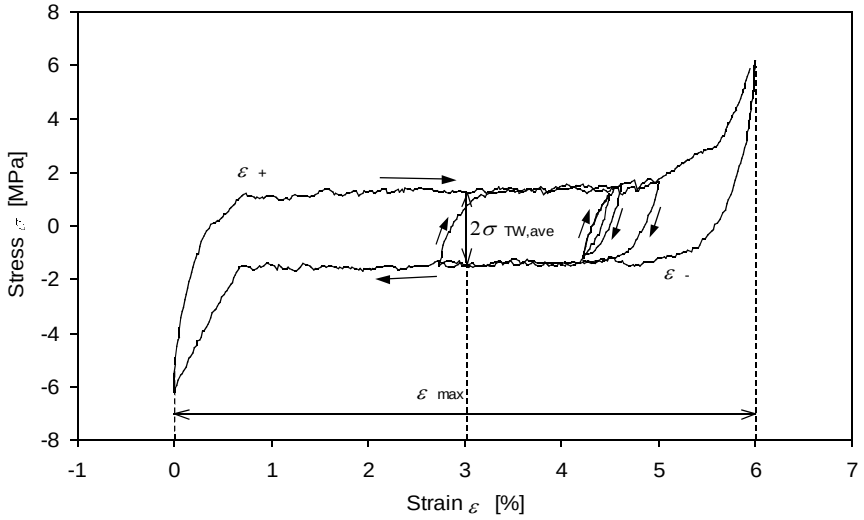

Fig. 8. Measured stress-strain loops of Ni-Mn-Ga in 5M martensite. The curves include boundary curves as well as the minor loop curves. The arrows indicate the direction of tracing.

3.1.3 Magnetization

The MSM materials are ferromagnetic and anisotropic. Therefore, the magnetization of the material is high, it has a certain saturation value, and depends on the direction of the applied field (see Fig. 2). The magnetization of the most utilized MSM material, Ni-Mn-

Ga in 5M tetragonal martensite, has been studied intensively [38,69,**P1**,30,**P2**,60]. The saturation value of intrinsic induction B_{is} has ranged from 0.6 T [30] to 0.68 T [**P2**] in different measurements. The saturation field strength H_s falls within in the range 520 kA/m [60] to 720 kA/m [30]. The relative permeability has also varied between different measurements. The relative permeability at low magnetic field strength in the ED varies from 4.5[30] to 100 [**P2**] and in HD from 1.7 [30] to 2.2 [**P2**]. Differences in these parameter values are most likely due to different compositions of Ni-Mn-Ga and possibly different annealing processes used for the studied samples. Annealing has a big influence especially on the permeability of the material [3]. In addition, the temperature has a significant influence on the magnetization curves of the material [13].

The anisotropy of the MSM material is important for its operation. The higher the anisotropy energy, the higher the MFI stress (see Eq. 4.6). This quantity has therefore been checked for many different compositions. With measurements, it has been shown that in Ni-Mn-Ga martensites anisotropy grows as a function of the lattice distortion [59]. In the 5M martensite, anisotropy is 150 kJ/m^3 and in 7M martensite 165 kJ/m^3 [32].

3.1.4 Operating temperature range

The operating temperature range is a very important parameter of the Ni-Mn-Ga MSM material. The MSM effect occurs in the martensite phase. So one limit for the operating temperature is the temperature range of the martensite. A key parameter is the temperature in which the martensite starts to turn into austenite, T_a. This temperature varies depending on the composition. The highest T_a temperature reported so far from a working Ni-Mn-Ga MSM material has been 67 °C [21]. For the martensite region, a lower bound has not been reported. Therefore, it does not limit the operating range from low temperatures. However, the MSM material can have different martensites in different temperatures, which affects the temperature range of an MSM application.

The saturation magnetization and the anisotropy energy of the MSM martensite grow when the temperature drops [12]. Also, the twinning stress in the material grows when temperature decreases [12]. This increase reduces the MSM effect. Therefore, the twinning stress limits the operation of the MSM material at the low temperatures. One

limit temperature is the point where the twinning stress is stronger than MFI stress. For one measured composition, this is about -160 °C [12]. Below this temperature the material does not show significant strains in the magnetic field. Usually for the actuator application the requirements are higher, because the actuator also has to work against other external forces. Therefore, the practical lower temperature limit comes at higher temperatures. Based on a measured temperature dependency curves of Ni-Mn-Ga [12], this limit temperature could be selected as -50°C . In sensor applications, it is not necessary to generate motion with MSM material in a magnetic field. For these applications, lower limit temperature for operation has not been reported. The same applies for different damping applications but at low temperatures, the material's twinning stress increases and changes the damping properties.

3.2 Measurement methods of magnetic and mechanic properties

Due to the large shape change property of MSM material, the measurement of magnetic and mechanical properties of MSM material needs special devices. The most interesting is to measure the magnetization, magnetic field strength, and mechanical stress and strain of the material. Sometimes, it is necessary to record all these simultaneously. In addition, the measurement system has to produce magnetic fields as well as mechanical stress to the material. The stress can be generated with a tensile testing machine and magnetic fields with electromagnet [56,55,**P1**,**P2**]. The stress can be measured with a load cell in the tensile testing machine and the strain with different types of position measurement instruments. When the element can change its shape during the measurement, the accurate sensing of magnetic field strength in the MSM element is difficult. This is due to the air-gap needed and the resulting demagnetization effect in the MSM material, i.e. the magnetic field inside the MSM element is smaller than the measured field outside the element.

Several types of measurement techniques for measuring the magnetization curve of ferromagnetic materials have been made [3]. The magnetization of MSM material is commonly measured with the Vibrating Sample Magnetometer (VSM), for example [62, 13]. The magnetic field strength can then be calculated using the demagnetization factor

and magnetic field measurement results outside the MSM element. This method needs the element to be vibrated and it cannot be done when the MSM sample is solidly connected with the stress and strain measurement. Shield [55] proposed a method, where the magnetization is measured with external Hall sensors. The Hall sensors were placed near the MSM element to measure the stray field caused by ferromagnetic material. He formulated an equation between the magnetization and the measured field in the external Hall sensor's. This made it possible to calculate the magnetization. Given the magnetization, the field strength can be calculated as in VSM method.

In this work, measurements of the properties of MSM materials were performed. The magnetization as a function of the strain [**P2**] as well as the magnetic field induced stress was measured [**P1**]. The magnetization of the material was measured using an AC method with two coils. One coil measured the flux density and the other the field strength in the MSM element. In this case, the problem of the demagnetization effect was avoided by placing the MSM element tightly between two high permeability ferromagnetic plates.

In the case of MFI stress measurement [**P1**], the MSM element size was changing and the element could not be placed solidly between the ferromagnetic plates. The field sensors were placed to a specific position next to the MSM element. The first one was used to determine flux density and the other field strenght. Due to the air-gaps, the field strength sensor measured a combined effect of field inside the element, H_{MSM}, and the stray field caused the demagnetization effect. The magnetic field strength in the material could only be determined with sufficient accuracy, when the material permeability was low.

4 MODELS OF THE MSM EFFECT

Several models for the MSM effect have been developed [18,45,30,27]. The main interest in the models has been related to calculating the MFI strain as well as the magnetization of the MSM material under external load and magnetic field. Approaches analyzing the MSM material as a bulk object or solving the detailed twin structure of the material have been proposed. For a model, two issues are important, the simplicity and accuracy. In this work, one aim has been to find a model in which the trade-off between the accuracy and simplicity is suitable for the application modeling.

James and Wuttig [18] and Tickle et al. [70] proposed a model to calculate variant distribution, from which the strain and magnetization of the MSM material can be solved. This model is based on minimization of the energy density in the MSM material. The model is numerical so that it does not give analytical formulas for the magnetization and strain. Since it solves the exact variant distribution in the MSM element, the demagnetization can be taken into account. Considering its detailed approach, the model should be the most accurate; however, the reported measured and calculated results differ from each other significantly. In addition, the lack of analytical result formulas reduces the usability of the model.

O'Handley [45] presented a model of the MSM material in which the MSM material element is studied as a bulk object, consisting of two variants. The basic idea of the model is to find the volume fractions of the variants of the material and then based on them calculate the MFI strain as well as the magnetization. Both magnetization and the macroscopic strain are assumed linearly dependent on the volume fractions. To solve the volume fractions, O'Handley formulated the equation for the free energy density in the material. This equation consists of magnetic energies, Zeeman energy and the magnetization energy of the reorientating variant as function of the rotation angle (see Eq. 2.10). Mechanically the material is assumed linear, the mechanical response to straining is taken into account with elastic energy. Later, the equation has been improved by the introduction of the external mechanical energy, which considers the external stress to the material [39]. A simplified hysteresis model between the magnetic field and strain was included in the main model [16,38]. The free energy density in one variant (sub

indexed i) can be written as

$$g_{\mathrm{i}} = -\mu_0 M_{\mathrm{i}} \cdot H + K_1 \cos^2 \theta_{\mathrm{i}} + \sigma_{\mathrm{int}} \cdot \varepsilon + \frac{1}{2} C \varepsilon^2, \qquad (4.1)$$

where C is effective stiffness, θ_{i} the angle between the magnetic field and the variant ED, and M_{i} the magnetization of the variant. Minimizing this energy, Eq. (4.1) for all variants gives the volume fractions of the variants. O'Handley also considered the effect of different energy conditions for the magnetization process in the material. The magnetization in the HD of a variant is interesting. If the anisotropy in the material is weak, the magnetization vector will rotate in the external magnetic field, but if it is strong, the material will reorient its unit cells (MSM effect). O'Handley also studied separately very high and medium size magnetic anisotropy. In the case of high magnetic anisotropy, he identified the driving force of the twin boundaries as the Zeeman energy (Eq. 2.7) difference between the two variants. Based on the assumptions, the driving force can be explicitly written as [45]

$$f = \mu_0 M_{\mathrm{s}} H \left[\cos\theta - \cos(\theta - \phi)\right], \qquad (4.2)$$

where θ is the angle between the applied magnetic field and the first variant ED, and ϕ is the angle difference between the variants. In the case of 5M martensite Ni-Mn-Ga, ϕ = 90º.

A similar energy density based model was proposed also by L'vov *et. al.* [27]. The explicit equations for the strain or magnetization as a function of the field strength were not written out but were described as a function of variant volume fractions. The magnetic susceptibility was also analyzed and an equation for the temperature dependence of the magnetization was given [27].

From the electromechanics point of view, the most promising modeling method of the MSM effect was introduced by Likhachev and Ullakko [30]. In this model, the effect of magnetic field is taken into account with the MFI stress, which will then cause the strain of the material. The MFI stress is solved using a Maxwell's relation [30]

$$\frac{\partial \sigma}{\partial H} = -\mu_0 \frac{\partial M}{\partial \varepsilon} . \qquad (4.3)$$

Eq. (4.2) gives the magnetic driving force moving the twin boundaries as a function of the angle at very low magnetic fields. In a general case, rather than being Zeeman energy difference (Eq. 4.2), the driving force is identified as the energy difference of the magnetic free energies per unit volume between the two variants [33]. This is equal to the internal energy (Eq. (2.6)) difference between the two variants. The most important magnetic driving force in Ni-Mn-Ga in 5M martensite is achieved when the material is magnetized in the HD direction of a variant. Given this condition, the driving force f moving the twin boundary can be written as

$$f = \mu_0 \int_0^H (M_a - M_t) dH . \qquad (4.4)$$

According to the Maxwell's rule (Eq. 4.3) the MFI stress can be presented as a function of the driving force [30,31]

$$\sigma_{mag} = \frac{f}{\varepsilon_0} = \frac{\mu_0}{\varepsilon_0} \int_0^H (M_a - M_t) dH . \qquad (4.5)$$

When the magnetic field strength is at saturation, $H = H_s$, the magnetic field induced stress is (see Eq. 2.9)

$$\sigma_{mag} = \frac{w_a}{\varepsilon_0} , \qquad (4.6)$$

where w_a is the anisotropy energy. Equation (4.6) shows that the MFI stress in the MSM material is proportional to the anisotropy energy and inversely proportional to the crystallographic limit strain. The accuracy of the MFI stress calculation formula (4.5) has

been proven by measurements using different MSM alloys, 5M martensite [**P1,** 41] and 7M martensite [32]. The measured numerical values of the stress are in 5M martensite 2.6 MPa, in 7M martensite 1.7 MPa and in nonlayered martensite 1.2 MPa [32,58].

The model developed by Likhachev *et al.* uses a principle, according to which both magnetic and mechanic forces will cause the same macroscopic deformation effects independent of the origin of the force [29]. The model explains the reason for the hysteresis between the magnetic field and strain (see Fig. 5) being in the twinning stress of the material (see Fig. 8)[29]. Since there is a need for initial stress before the material gives significant strain, there is a critical field strength corresponding to the start of rapid growth, the switching field H_{SW} (see Fig. 5) [12]. This parameter depends on the strain value of the material as well as temperature.

The twinning stress in the material is opposing the movement of the twin boundaries in a non-linear way (see Fig. 8). In a static case, the twinning stress (or the total magneto-mechanical stress) σ_{TW} in the MSM material is the difference between the MFI stress σ_{mag} and the opposing external mechanical stress σ_{mech} [33]

$$\sigma_{TW} = \sigma_{mag} - \sigma_{mech}. \qquad (4.7)$$

The strain of the material depends on the stress-strain relationship of the MSM material (see Chapter 3). If the opposing mechanical stress σ_{mech} is too strong, the material does not give a full MFI strain [15,38]. For an accurate calculation of the strain, the mechanical hysteresis (see Fig. 8) has to be modeled.

The model developed by Likhachev et. al. interprets the strain of the MSM material as function of the magnetic field strength and external stress with good accuracy. The stress-strain response in the material, i.e., the twinning stress (Fig. 8), can be measured mechanically and used in the calculation of the MFI strain (Fig. 5) [29]. The model needs only a limited amount of input data, so it is simple. Due to these reasons, this method was chosen for the MSM application models in this study.

An approach using the MFI stress has been used also by Müllner *et al.* [44]. The material produces shear force, which results in the macroscopic stress. Müllner *et al.* proposed a model of the MFI shear [40], which was later detailed for macroscopic stress

[44]. Just as with the model by O'Handley, the system is based on the magnetic energy expressions on both sides of the twin boundary in the MSM material. The simplified magnetization curves are assumed (see Fig. 2b). The resulting MFI stress calculation formula has two magnetization parameters, which are the anisotropy energy, w_a, and the saturation magnetization, M_s [41]

$$\sigma_{mag} = \begin{cases} \frac{\mu_0 M_s H}{\varepsilon_0}\left(1 - \frac{\mu_0 M_s H}{4 w_a}\right), \text{when } H < H_s \\ \frac{w_a}{\varepsilon_0}, \text{when } H \geq H_s \end{cases} . \qquad (4.8)$$

This formula can also be derived with the more general Eq. (4.5) proposed by Likhachev *et. al.* Equation (4.8) is useful, since the magnetization characteristics of MSM material are such that usually this type of two parameter model gives correct functional dependence for the MFI stress. In order for Eq. (4.8) to be valid, the permeability at low magnetic fields in ED must be high. A three-parameter model for MFI stress has also been proposed, which does not make that assumption [61].

4.1 Influence of the external field direction to the MSM effect

One benefit of the model developed by O'Handley is that it takes into account the different directions of the external magnetic field in the MSM material. In the case of a very high magnetic anisotropy, the effect of the direction of the external magnetic field has been studied [45,17]. On the basis of Eq. (4.2), the maximum driving force for the twin boundary is achieved, when the angle between the external magnetic field and the ED of the other variant is 45º. However, the results only apply to the low magnetic fields and to a constant magnetization vector. In practice, the twin boundary motion does not occur at low magnetic fields.

Mullner *et al.* extended this consideration for the MFI shear in the case of more general magnetic field energy [10]. They derived the field direction dependence of the MFI shear in saturation field H_s. Based on this equation, the MFI stress in saturation condition ($H > H_s$) is

$$\sigma_{\mathrm{mag}} = \frac{K}{\varepsilon_0}\cos 2\theta . \qquad (4.9)$$

The equation predicts that the maximum MFI stress is achieved, when $\theta = 0°$ or $\theta = 180°$, i.e. when the magnetic field is parallel to HD of the other variant. This result is in accordance with the most obvious conclusion based on the unit cell orientation difference between the variants (90°). Even though these angle dependencies have been proposed, only a very limited number of measurements have been made to confirm the assumed effects.

4.2 Efficiency of the MSM material

The work output and coupling factor between the mechanical and magnetic energies of the MSM material are important operation parameters. Some simplified equations for calculating the work output have been proposed [33,45]. The most detailed analysis was done by Likhachev *et al.* [33], who calculated the mechanical hysteresis curves of the 5M martensite MSM material during a full-operation cycle of the material. The energy balance can be solved from the cycle curves. The energies related to the cycle are the input magnetic field energy density, w_{mag}, output mechanical energy density, w_{mech}, and loss density, q. Nearly all the losses are caused by the mechanical hysteresis and only this was considered. The energy conservation principle gives the energy balance and coupling factor, η_{MSM}, between the magnetic field energy and the mechanical energy as [33]

$$w_{\mathrm{mag}} = q + w_{\mathrm{mech}}, \qquad (4.10)$$

$$\eta_{\mathrm{MSM}} = w_{\mathrm{mech}} / w_{\mathrm{mag}}. \qquad (4.11)$$

The shortcoming of this method for solving the coupling factor is the difficulty in calculating the mechanical hysteresis loops and the lack of an analytical result. By making simplifications for the stress-strain hysteresis, an analytical equation for the

coupling factor can be derived assuming the material performs a full cycle (strain $\varepsilon = \varepsilon_{max}$) [66]. Figure 9 shows simplified mechanical hysteresis loops for the case, when MSM material is in saturation magnetic field, and when it is not in the magnetic field. Without the magnetic field, the mechanical hysteresis loop is positioned around the strain axis, as in the measured curve in Fig 8. When the material is exposed to the magnetic field, it lowers the mechanical hysteresis loop by value σ_{mag} (see Fig 9). Let's study one cycle of the MSM material. The starting point is at A in Fig. 9. A contracting mechanical stress is applied to the element and the state of the material moves to point B on the stress-strain diagram. Then a magnetic field is added and simultaneously magnitude of the contracting mechanical stress is increased (the stress value decreases) so that the strain stays constant. As a consequence, the state of the material moves to point C. Then contracting mechanical stress is released and the state moves first to D and then to E and finally to the starting point A. During this cycle, the material gets the energy density caused by magnetic field, $w_{mag} = \sigma_{mag}\ \varepsilon_{max}$, and gives out the mechanical energy density $w_{mech} = \sigma_{mag}\ \varepsilon_{max} - 2\sigma_{TW,ave}\ \varepsilon_{max}$. The formula for the coupling factor between the magnetic field energy and the mechanical energy is [66]

$$\eta_{MSM} = \frac{w_{mech}}{w_{mag}} = \frac{\sigma_{mag} - 2\sigma_{TW,ave}}{\sigma_{mag}}. \qquad (4.12)$$

Using Eq. (4.12), we can solve the efficiency of the materials with different twinning stress values. For example with the values corresponding to Fig. 9, $\sigma_{TW,ave}$ = 0.7 MPa and σ_{mag} = 3.0 MPa, the coupling factor has the value η_{MSM} = 53 %. Equation 4.12 demonstrates the importance of the twinning stress parameter $\sigma_{TW,ave}$ to the efficiency of the material.

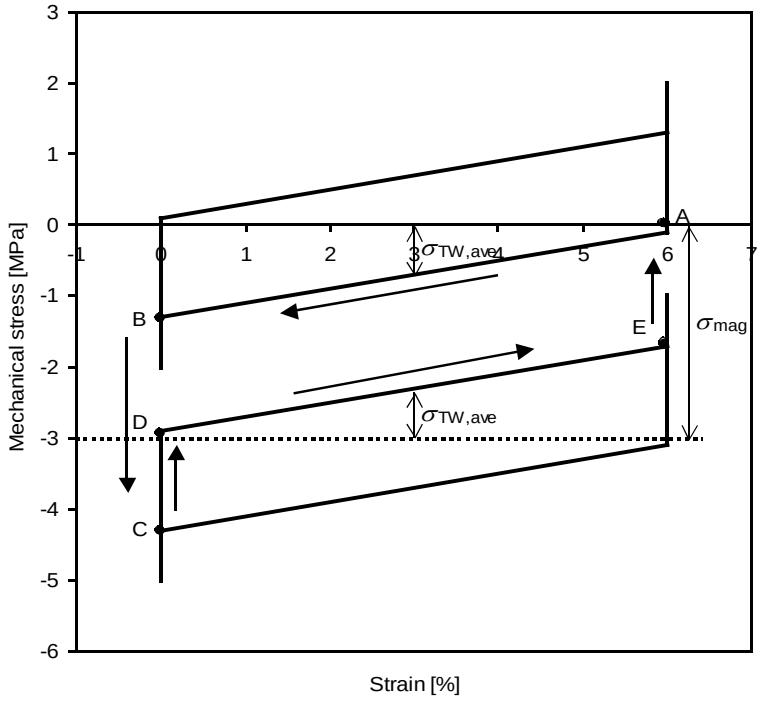

Fig 9. Simplified mechanical hysteresis curves with and without external magnetic field. The positive values of mechanical stress correspond to elongating stress and negative values to contracting stress. The arrows desribe the movement of the mechanical stress-strain state during the studied process.

4.3 Magnetization model of MSM material

In this work and in the following text, the models for the magnetization of 5M martensite Ni-Mn-Ga are presented. Due to the different variant structure, the presented models are not necessarily valid for other MSM materials.

The magnetization of a material is described by a magnetization curve (see Chapter 3). Besides the magnetic field strength dependence, the magnetization in MSM material also depends on variant volume fractions and variant distribution. In fact, the magnetic field strength and flux density do not have a constant value inside an MSM element

consisting of different variants. However, for the simplicity, the material is considered homogeneous and only one field value is used to represent the magnetic state. The magnetization M_{MSM}, field strength H_{MSM} and flux density B_{MSM} are called the effective values of the magnetic fields inside the material [**P3**]. These are the average values of the magnetic fields inside the MSM element and take into account the real non-homogeneity of the material. The effective field values are used in the application modeling.

The MSM elements can be trained so that they consist only of two differently oriented macroscopic variants. The volume fraction of the first one is x and the second one 1 - x. Since the external magnetic field is usually placed along the ED of the other variant, the magnetization in this direction is important. O'Handley presented the relative effective magnetization $m_{rel} = M_{MSM}/M_{sat}$ in the direction of the ED of the first variant as a function of variant volume fractions $f_1 = x$ and $f_2 = 1 - x$ [45]

$$m_{rel} = f_1 + f_2 \cos\phi , \tag{4.13}$$

where ϕ is the angle between the second variant magnetization and the external magnetic field. In this case, the simplified magnetization curves (See Fig. 2b) are assumed and the term $\cos\phi$ in Eq. (4.13) represents the HD rotating magnetization process of the second variant. Besides the variant areas, the material consists of different domain areas (see Chapter 3). As with the variant volume fraction x, the domain volume fraction α_p can be explicitly written out. Hirsinger et al. presented the magnetization vector **M** in form [17]

$$\mathbf{M} = M_s\left(2\alpha_p - 1\right)\left[x\mathbf{u}_x + \left(x-1\right)\mathbf{u}_y\right], \tag{4.14}$$

where $\mathbf{u}_x$ and $\mathbf{u}_y$ are the unit vectors parallel to the ED of the unit cells of two variants. The variant volume fraction x defines the strain ε of the MSM material, $\varepsilon = x\ \varepsilon_0$, where ε_0 is the CLS. Therefore, the variant volume fraction dependence can be seen as a strain dependence. The models by Likhachev *et al.* and O'Handley (Eq. 4.13) both assume a linear dependence of magnetization on strain. The linear dependence results from the assumption that the magnetic regions in the MSM element are in parallel to the external magnetic field and the magnetic field strength H_{MSM} is constant in the whole element.

Based on the variant distribution in the element (see Fig. 4), this is not obvious. The model developed by Wuttig *et al.* takes into account the demagnetization effect in the MSM element, but it does not give an analytical result for the magnetization. With the linearity assumption, the effective magnetization M_{MSM} in the HD direction of the other variant can be written as [30]

$$M_{\mathrm{MSM}}\left(H_{\mathrm{MSM}}\right)=M_{\mathrm{a}}\left(H_{\mathrm{MSM}}\right)+x\left[M_{\mathrm{t}}\left(H_{\mathrm{MSM}}\right)-M_{\mathrm{a}}\left(H_{\mathrm{MSM}}\right)\right], \tag{4.15}$$

where $M_{\mathrm{a}}(H)$, $M_{\mathrm{t}}(H)$ are the magnetization curves in ED (axial direction) and HD (transverse direction). Equation (4.15) is a more general form of magnetization than Eq. (4.13) and any assumptions on the magnetization dependence on the magnetic field strength in HD or ED can be included. Based on Eq. (4.15), we can write the effective permeability μ_{MSM} of the material as

$$\mu_{\mathrm{MSM}}=\mu_{\mathrm{a}}+x\left(\mu_{\mathrm{t}}-\mu_{\mathrm{a}}\right), \tag{4.16}$$

where μ_{a} is the permeability in ED and μ_{t} the permeability to HD. Solving an exact solution based on the structure of the material is difficult, since one requires detailed information on the variant distribution in the MSM element. It is difficult to achieve. In this study only extreme case analysis has been performed. The linear dependence (Eqs. 4.15, 4.13) follows from the assumption that the internal areas in the MSM element are in parallel. The other extreme is to assume that they are in series. In the serial case, the magnetic flux density is constant and the effective field strength, H_{MSM}, in the MSM material [**P2**] can be solved with the Ampere's law

$$H_{\mathrm{MSM}}\left(B_{\mathrm{MSM}}\right)=H_{\mathrm{a}}\left(B_{\mathrm{MSM}}\right)+x\left[H_{\mathrm{t}}\left(B_{\mathrm{MSM}}\right)-H_{\mathrm{a}}\left(B_{\mathrm{MSM}}\right)\right], \tag{4.17}$$

where H_{a} and H_{t} are the magnetic field strength in ED and HD. If assuming constant permeabilities in HD and ED, the effective permeability, μ_{MSM}, of the element is written as [**P2**]

$$\mu_{\mathrm{MSM}} = \frac{\mu_{\mathrm{a}}\mu_{\mathrm{t}}}{\mu_{\mathrm{a}} + x(\mu_{\mathrm{t}} - \mu_{\mathrm{a}})} \ . \tag{4.18}$$

Since the effective magnetization dependence on strain is not linear, this can be called the non-linear model as opposed to the linear model of Eqs. (4.16,4.15). In this work, the magnetization dependence on the strain was studied with measurements from 5M martensite Ni-Mn-Ga. It was found that the dependence is linear at higher magnetic field strength values, but at lower field values the dependence is nonlinear, though, not exactly according to Eq. (4.18) [**P2**]. This could be expected, since the Eq. (4.18) represents an extreme case.

5 MSM ACTUATORS

MSM actuators are devices that produce the magnetic field for the MSM element, which in turn generates the mechanical motion. An MSM actuator usually consists of an MSM element, a ferromagnetic core, and coils [68,2]. Air-cored actuators have been made, too [36]. The benefit of an air-cored actuator is its small size, but the air-core actuator needs high currents to generate the magnetic field. So far, the most common actuator type has been a linear axial motion actuator [2,68]. In this study 5M martensite Ni-Mn-Ga alloys have been used in the actuators. A schematic view of this type of actuator structure can be seen in Fig 10. To minimize the magneto-motive force needed, the magnetic field is usually applied to the MSM element in the transverse direction in relation to the direction of the output mechanical motion. The MSM elements in the actuator consist of two variants, one has ED along the magnetic field and the other one along the mechanical stress. This maximizes the MFI stress in the material (see Eq. 4.9). The overall construction produces a MFI stress to the MSM element to elongate itself in magnetic field.

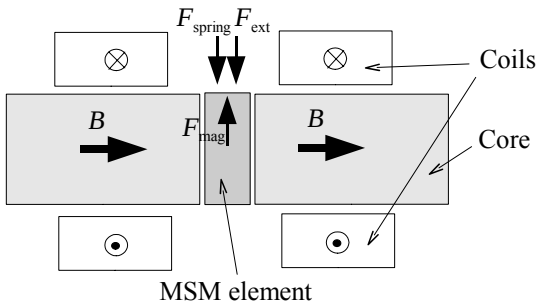

Fig. 10. Schematic view of the structure of a commonly used MSM actuators. The opposing forces against the MSM element are spring force F_{spring} and external force F_{ext}, while the MSM element itself generates MFI force F_{mag}.

The twinning stress in the MSM material maintains the strain value, when external forces and magnetic fields are removed. Since the motion of the material is not reversible by itself, opposing loads are needed to move the MSM element backward. In pre-stressed actuators Fig. 10, the required opposing loads are realized with springs. It is also

possible to use two reverse-coupled MSM actuators to move the elements of each others in opposite direction [22,7]. With this construction a spring load is not necessary for the reversal operation of the actuator. An extra benefit of this two-actuator system is that the material does not need any energy to maintain its position and the system can resist fairly high disturbance forces.

Besides using the opposing mechanical loads, the actuator can use magnetic fields in two directions to make a reversible movement actuator system. If the field is applied in the first direction, it elongates the element. The reverse movement is induced with transverse directional field. An actuator construction based on two field directions has been tested for a pump application [**P5**].

Due to the twinning hysteresis, the opposing mechanical stress has a certain value or range of values for the maximum reversible output strain of the material [28,68]. This optimal value for the opposing stress depends on the twinning stress. If the twinning stress is low, the output strain is high, but if the twinning stress is high, the output strain is low. The twinning stress defines the limits for the MSM material used in actuators. If the actuator gives only one-directional movement, the twinning stress has to be smaller than the MFI stress, $\sigma_{mag} > \sigma_{TW}$. Usually, the actuators are made so that the element movement is two directional. In this case, the material demand is even higher, $\sigma_{mag} > 2\sigma_{TW}$.

Permanent magnets can be used in an MSM actuator, which is then called a permanent magnet (PM) biased actuator [**P3**]. Usually, a PM actuator is constructed so that the permanent magnet generated DC field is half of the maximum magnetic field needed. In this way, the supply current of the actuator is symmetric. The use of permanent magnets reduces the electrical losses in the actuator, because a smaller field needs to be generated with the current for the operation of the actuator. An additional benefit of the PM biased MSM actuator is that the position can be maintained without current even in a pre-stressed actuator [67]. This is due to the mechanical hysteresis of the material. In some applications, maintaining the position reduces losses considerably.

The total MFI force generated by the MSM material depends on the cross-section area of the element. The stroke is defined by the length of the element. These conditions also affect the size of the actuator: a long actuator gives a high stroke and an actuator

with a large cross-section gives high output force. Figure 11 shows some example actuators manufactured by Adaptamat Ltd.

Besides the axial linear motion, the use of shear [39] and bending [25] actuation has been reported. Kohl *et. al.* has described a bending type actuator using Ni-Mn-Ga [25]. In this actuator, the MSM element bent in martensite due to the magnetostatic force. A force caused by the shape memory effect was used to straighten the element. Large bending angles, up to 120º, were demonstrated [25].

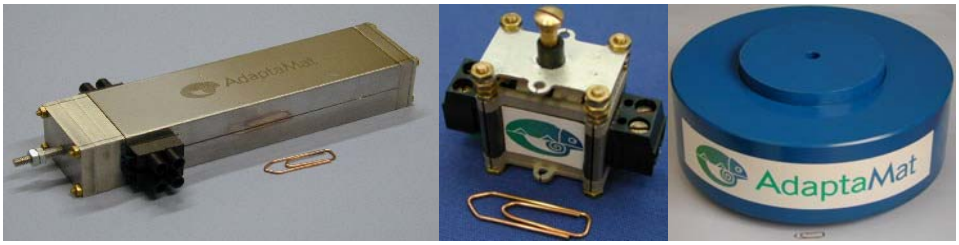

Model: A5-2 Model: A06-3 Model: A1-2000

Model	Size [mm]	Frequency [Hz]	Blocking force [N]	Max. stroke [mm]
A5-2	20×30×120	DC...300	3	5
A06-3	11×23×21	DC...1000	3	0.6
A1-2000	∅260×90	DC...100	1000	1

Fig. 11 Example MSM actuators and their basic operation parameters [1]. Symbol ∅ describes the diameter of the actuator.

5.1 Modeling and control

The main aim in modeling an MSM actuator is to calculate the output strain and stress as a function of the input current and external stress. In this work, the modeling has been done in static condition. The studied models of an MSM actuator consist of many sub-models. These include a model of the MSM effect, a model for mechanical response and models for the magnetic, electric and mechanical circuits of the actuator. In this work, the MSM effect was calculated using the equations presented by Likhachev *et al.* (see Chapter 4). A key parameter of their model, the MFI stress, is defined by the magnetic

field strength H_{MSM} (see Eq. 4.5). The field can be solved by modeling the magnetic circuit of the actuator. In this work, simple reluctance network models of the magnetic circuits of MSM actuators were developed [**P6**,**P3**]. Similar models have been made for magnetostrictive material actuators [8] as well as for electrical machines. The main aim has been to describe the linear axial motion actuator. Based on a developed model of a non-permanent magnet MSM actuator, the magnetic field strength H_{MSM} can be written as [**P6**]

$$H_{\mathrm{MSM}} = \frac{\frac{R_{\mathrm{m1}}}{R_{\mathrm{mC}}} Ni}{w(1-\varepsilon) + \mu_{\mathrm{MSM}} A_{\mathrm{side}} \left(R_{\mathrm{m1}} + R_{\mathrm{mG}}\right)}, \tag{5.1}$$

where R_{m1}, R_{mC} and R_{mG} are magnetic reluctances of the actuator, N is the number of turns, i the current, w is the width of the MSM element, and A_{side} the side cross-section area of the MSM material (See reference [**P6**] for more details). Equation 5.1 demonstrates that the magnetic field strength in the MSM element is proportional to the current of the actuator. Therefore, the supply of the actuator is useful to be operated in current control mode [**P5**]. The actuator can also be driven as a voltage controlled system, but this causes delays in the operation of the actuator. Beside the field strength, the MSM material strain also depends on the external load on the element. In addition, the stress-strain relationship and the MFI stress are dependent on the temperature. If the position of the actuator is to be controlled, an extra control loop including a position sensor is necessary [**P5**]. A position control system diagram is visible in Fig. 12.

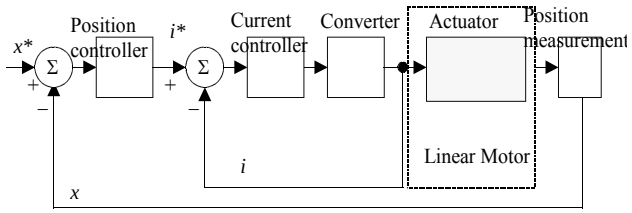

*Fig. 12. A position control system of an MSM actuator [**P5**]. In the figure x* is target position, x measured position i* target current and i measured current.*

The mechanical circuit of the actuator in the static case can be modeled using Eq. (4.7). This takes into account the twinning stress as well as the effect of the external mechanical stress, which is necessary for accurate calculation. The spring load of a prestressed actuator is included as part of the opposing mechanical force [**P6**].

Even though only the static case modeling has been tested, some points of the dynamic modeling can be made. In most applications, the eddy currents do not significantly influence the operation of the actuator [36]. It can be assumed, therefore, that the most significant factor for the dynamic slowness is caused by the moving mass. The model built by Lihachev *et al.* indicates a straight forward method of dynamic modeling: the difference between the MFI force and the opposing mechanical force is accelerating the moving mass, m. Based on this assumption and Newton's second law, the strain ε can be solved from

$$\left(\sigma_{\mathrm{mag}} - \sigma_{\mathrm{mech}} - \sigma_{\mathrm{TW}}\right) A_{\mathrm{Cross}} = ml\,\frac{d^2\varepsilon}{dt^2}, \tag{5.2}$$

where A_{cross} is the cross-section area and l_z the length of the MSM element.

In the developed models, sensitivity to the variation of the parameter values has not been studied, but, based on the equations, it is obvious that some parameters in the model affect the results significantly. Small changes in parameters like the air-gap lengths may cause big changes in the predicted stroke of the actuator. In the case of modeling a ready made actuator, it is efficient to measure a few example strain curves and fit the parameters so that the calculated results are in accordance with the measured ones.

5.2 Operating parameters and applications

The advantages of the MSM actuators consist of large strains, short rise time and damping abilities. Actuators with a stroke of up to 5 mm and actuators with a force of up to 1 kN have been built (see Fig. 11). So far, no limit, practical or theoretical, for the size of stroke or force of actuators has yet been reported. From MSM actuators with a ferromagnetic core, accelerations of up to 5000 m/s^2 and speeds of up to 1.5 m/s have been measured [**P4**]. In the case of an air-core and fast current pulses, even higher

acceleration values can be achieved [36]. The rise time of the actuator depends on the stroke and the moving mass. This kind of high acceleration makes it possible to use the actuators at very high frequencies of up to several kHz. The fatigue life of an actuator was also studied in this work. Measurements demonstrated, that $200 \cdot 10^6$ moves can be made with no significant reduction of the strain of MSM material [68].

The mechanical hysteresis (see Chapter 4) leads to power dissipation (internal friction) in the cyclic applications. This reduces the mechanical vibrations and the effect of current high harmonics. The negative sides of the twinning stress is the losses and hysteresis between the control current and the strain.

So far the main temperature limitations of the MSM actuators are defined by the temperature limits of the MSM material discussed earlier (see Chapter 3.1).

In some applications, it is beneficial to amplify the mechanical motion of the MSM material. This can be realized with a linear motor consisting of an MSM actuator and two electromechanical clamps. Two different linear motors were built during this work **[**22, **P5]** (see Fig. 13). The motor operates following the inchworm principle and moves the sliding shaft on top of the actuator. Up to 80 mm/s of average speed from this type of linear motor construction has been measured [22]. The speed was limited by the speed of the magnetic clamps and length of the motion cycle. The developed linear motor can be used as a positioning device. The positioning accuracy of this motor was high, up to 1μm was measured **[P5]**. The construction was robust and it is likely that even better results could be reached. The theoretical limit for positioning accuracy in MSM material is the shape change in the deformation of a single atomic layer. This is close to a 1 pm.

Only limited studies have been reported on the efficiency of the MSM actuator. The losses in the MSM actuator are caused by losses in the core, coil and in the MSM element. The main cause of the losses in the MSM element is the twinning stress in the material. A simple equation for the coupling factor between the magnetic energy and mechanical work has been determined (see Chapter 5.2). The losses of the actuator depend strongly on the actuator size and construction. The overall losses in the MSM actuators can be very low. An actuator operated with DC current giving 0.2 mm stroke and 1N force with peak losses of 5 mW has been built [67].

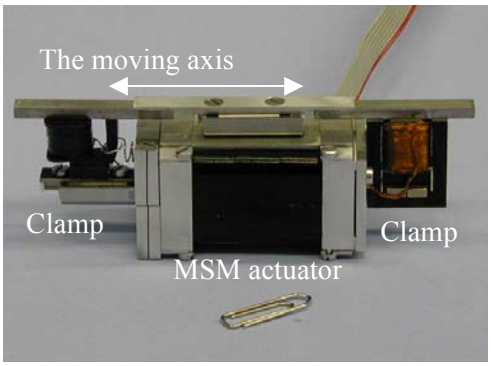

Fig. 13. Photo of the built MSM linear motor.

A large set of different types of applications for the MSM actuators**,** for example, proportional valves, positioning devices and vibrators, have been proposed [**P5**,20,1**]**. The benefits of the MSM material, high strain, control and damping abilities affect the potential applications of the actuators. Like many other active materials, the MSM material has the benefit of making mechanical systems simpler [20].

6 MSM SENSORS

All active materials also have a reverse effect, which can be used in different types of sensor applications. The most commonly utilized are the piezoelectric sensors, which are commercially used in various applications, load cells, for example, or acceleration sensors. The use of magnetostrictive materials for sensing position has been studied as a separate application [76] and as part of a magnetostriction actuator [26]. Magnetostrictive material has also been used as a voltage generator [34]. Generally, magneto-elastic materials can be employed as sensing elements in displacement, torque or force sensors [49]. MSM material can be used as a sensor, too. The material can be used for position, velocity or acceleration sensing. One benefit of an MSM sensor compared to the other active material sensors is the possibility for large displacements. This is due to the high strain of the MSM material.

Since for sensor applications only low magnetic field is necessary, the construction has more freedoms than in the case of an MSM actuator. However, in this work as well as in other published results, the tests for sensing applications have been performed with constructions similar to actuators (Fig. 10). The magnetic field is applied orthogonally to the mechanical movement and the position [43,64,63], velocity [**P3**] or acceleration are measured as a function of magnetization [43], voltage [**P3**] or inductance of the actuator [63], thus resulting in the mechanical parameters to be sensed with magnetic or electric variables. Since the construction of the MSM sensors is the same as in actuators, similar models have been used (see Chapter 5.1). The magnetic circuit has been modeled with the lumped parameters and connected with the mechanical and electric circuits [**P3**]. The strain dependence of the magnetization is crucial for sensor applications [**P2**] (See Chapter 4.3). The magnetization dependence on strain was found to be non-linear in the low magnetic fields (< 40 kA/m) and linear at higher fields [43, **P2**]. Therefore, using high fields would give a better response for a sensor. However, in practice, the need to generate a high magnetic field is often a big shortcoming and so it is wise to use MSM sensors with low magnetic fields, regardless of the non-linearities.

As the magnetization depends on the strain of the MSM material, the most obvious sensor application is a position sensor. This can be implemented by measuring the

magnetization [43] or properties related to it, like inductance [64, 63]. In addition to the linear position measurement, the material can also be used in sensing the other deformation modes. The MSM material is soft and the bending mode makes it possible to use it in a joystick application [64]. When the element is bent, one side of the element has a higher permeability than the other. This can be monitored with field sensors on both sides of the actuator.

Besides the position monitoring, the MSM material can be used to measure the shape change speed. The material affects the magnetic flux going through the element and due to Faraday's law, the change in flux can be monitored from induced voltages [**P3**]. Since the induced voltages are proportional to the time derivative of the flux change, this phenomenon makes a speed sensor application possible. The measured results show a linear or close to linear relationship between the induced voltage and the velocity [**P3**]. The induced voltages can also be used directly for power or voltage generation. Considerably high voltages (close to 100V) were measured from the test application during this work [**P3**].

The MSM material gives strain only after it is exposed to a certain stress (see Fig. 8). If a mass *m* is placed on the element, under dynamic conditions, a certain acceleration will cause a shape change in the material. This phenomenon can be used to generate a limit acceleration sensor from MSM material [64].

7 DISCUSSION

The MSM material is a new material type. Properties of the material have been under research through the last few years. However, the applications of the material have not been studied with the same intensity. The aim of this study has been to investigate the material applications as well as the material properties related to the applications. In addition, the models of the material applications, sensors and actuators, have been made. The most promising MSM alloy for the applications has been found to be the 5M martensite Ni-Mn-Ga. Therefore, this alloy type, together with the applications using it has been the main interest of this study.

Many models for the MSM material have been made prior to this work. However, since the material is new, the models have not yet been fully investigated. A model introduced by Likhachev and Ullakko [30] includes equations for calculating the MFI stress and strain of the MSM material. The accuracy of this model has been partially checked with measurements. The model is simple and general magnetization curve dependencies as well as mechanical characteristics can be included in it. Therefore, it was selected as a basis of the application modeling. The accuracy of MFI stress calculation [**P1**] and the magnetization dependence on the strain [**P2**] were measured from 5M martensite Ni-Mn-Ga material in this study. Both these properties are an important part of the material model. The MFI stress measurement is difficult, especially when the measured magnetic field strength is inaccurate. This is due to the demagnetization effect in the MSM material. The measurement method for the MFI stress determination in a magnetic field was further developed in this study. Similar ways of measurement have been used before [21,41]. With the described method, the accuracy of the field strength measurement is still no more than sufficient and results have to be achieved under specific conditions.

In principle, for the accurate modeling of the material, the variant distribution should be known in detail. However, this can be difficult to achieve. Some elements have more twin variants, while others have fewer. The reason for this is so far unclear. In addition, the measurement of properties like magnetization curves of a part of the material is very hard. The solution for these problems is to use average values, which take into account

the different regions in the non-homogeneous material. The averaging method simplifies the model of the material. In addition, the approach seems to give good agreement between the calculated and measured strain and stress results. These variables are not significantly dependent on the exact variant distribution in the MSM element. On the other hand, parameters like the magnetization of an element depend on the distribution.

The magnetization dependence on strain is important for the calculation of motion generation and, especially, for the sensor application modeling. Therefore, the strain dependence of magnetization was measured in this work [**P2**]. The measurement was done with AC method and both field strength and flux density were measured with coils. Again, the demagnetization effect caused problems for the measurement of the magnetic field strength. The problem was solved by placing the MSM element between high permeability MSM plates during the measurement. Several magnetization curves were measured at different fixed MSM element size. The dependence on strain can be solved from this set of curves.

In material models, the magnetization has been assumed linearly depending on the strain. The measured results achieved in this work showed that the previously proposed linear dependence is valid in high magnetic fields. However, in lower magnetic fields (H_{MSM} < 40 kA/m) the magnetization strain dependence is non-linear. The non-linear region is connected to the field strength value of the "knee" of the magnetization curve, which depends on strain. It is likely that the dependence could be calculated by knowing the exact internal region distribution in the MSM element. In this work, only a simple limit condition was proposed based on the simplified assumption that the regions are in series with respect to the external magnetic field. The approximation did not give quantitatively accurate results but the measured curve was similar to the approximation. The non-linearity result is important information for the sensor applications of the MSM material because it is beneficial to operate them in low magnetic fields.

The actuator and sensor models were developed using the MSM material model made by Likhachev and Ullakko [30]. Besides the material behavior, the main issue in the modeling of the MSM actuators or sensors is about calculating the magnetic fields in the devices. Since the structure of both the actuators and sensors is similar, the same models can be used for them. Prior to this work, complete models, including the magnetic circuit of MSM applications have not been published. In this work, lumped parameters have

been used for modeling the magnetic circuit of the actuators and sensors [**P3**,**P6**]. Models have been made for the applications with [**P3**] and without permanent magnets [**P6**]. The coupling between the magnetic and mechanical circuit has been developed by Likhachev *et al.* [33], which was used in the present work. The modeling of the electric circuit connected to the MSM devices has been very limited. Detailed calculation of the current has not been performed in this work. The electric circuit is taken into account only with current of the coils. In reality, the MSM element causes changes in the magnetic circuit and therefore also affects the current of the actuator. In static cases, this influence does not exist. Besides the study of induced voltages, only the static case has been modeled during this study.

The linear magnetization dependence on the strain of MSM material has been demonstrated as a separate application prior to this work [43]. In this work, the reverse MSM effect was used in voltage generation for the first time [**P3**]. When the MSM material is subjected to short mechanical impulses, its magnetization changes. In the study, this effect was used to generate voltage using a Ni-Mn-Ga MSM material placed inside a PM biased MSM actuator. The induced voltage depends on the geometrical and material parameters of the MSM actuator, as well as on the speed by which the MSM material changes its shape. The described method and system can be used in voltage or power generation.

Using the developed magnetic circuit model, it is possible to calculate the induced voltages. The results calculated from the model were compared with the experimental ones. Generally, modeling of the induced voltages has difficulties, due to the strong sensitivity to the input parameters. However, in this study the modeling results demonstrated sufficient accordance with the measurements. In addition, the induced voltages were proportional to the speed of the MSM material, thus the device can also be used as a speed sensor.

Another application type built during this work was a linear motor [**P5**]. Two different linear motors were built. Both of them operated on an inchworm principle. The designs consist of MSM actuator and two clamps. When these three components are operated in a specific pattern, an amplified motion of the MSM actuator can be generated. For the linear motor, a control system was built, too. The same system can also be used for an actuator. In this work, it has been stated that the actuator works better

in a current control mode rather than in voltage control mode, because the field strength inside the actuator is closely proportional to the current and in the same phase as the current.

Many MSM material properties have been measured before. In this work, speed, acceleration and the fatigue life of a high-permeability MSM actuator has been studied with measurements [**P4**]. Another property measured during this study has been the positioning accuracy. This was studied from a linear motor [**P5**].

8 CONCLUSIONS

MSM materials form a new material type with interesting properties. The possible applications are in the field of motion generation and sensoring. In this work, both of these have been studied. To understand the operation of the MSM applications, the properties of the material itself have to be known. As a part of this thesis, the magnetization dependence on the strain was studied. The MFI stress of the MSM material was measured, too. For both cases, specific measurement set-ups were planned and measurements were made. The measured MFI stress had a good agreement with theory, but the magnetization dependence on strain is not totally clear. In low magnetic fields, only estimation formulas can be used. More accurate calculation formulas may have problems unless the exact internal structure of the MSM element is known.

The structure of an MSM actuator and sensor and the basic reason for operation have been presented. Many operation parameters of the MSM actuators have been measured during this work: speed, acceleration, positioning accuracy and fatigue life.

Several MSM material models have been made prior to this work. These were studied and one of them was selected for the actuator and sensor models. The structure of an MSM actuator and sensor are similar to each other. Therefore, their models are very similar. A complete model for the MSM actuator and sensor have been developed and presented, with and without permanent magnets. The accuracy of the selected model has been found sufficiently good, even though differences between the measured and the calculated results exist. Based on the results, it is likely that all significant physical phenomena in actuators and sensors have been taken into account. The sensitivity of the model has not been studied, but some parameters of the model significantly influence the calculated results.

For this thesis, new MSM applications were made, namely a velocity sensor or a voltage generator and two linear motors. The linear motor control system was designed and built for position control. The positioning accuracy of the linear motor was found to be good even in a robust construction. The physical background of the velocity sensor was described in detail and a model for calculating the induced voltage was presented. The dependence between the velocity and induced voltage was also proven with

measurements.

References

[1] http://www.adaptamat.com

[2] Aaltio I. and Ullakko K., "Magnetic Shape Memory Actuators", Proc. of Actuator 2000 conference, 19-21 June 2000, Bremen, Germany, pp. 527-530.

[3] Bozorth R.M., "Ferromagnetism", D. Van Nostrand Company, New York, 1951, p. 968.

[4] Carlson J.D., Stanway R., Johnson A.R., "Electro-rheological and magneto-rheological fluids: a state-of-the-art report", Proc. of Actuator 2004 conference, 14-16 June 2004, Bremen, Germany, pp. 284-288.

[5] Chernenko V.A., Cesari E., Kokorin V.V., Vitenko I.N., "The development of new ferromagnetic shape memory alloys in Ni-Mn-Ga system", Scripta Metallurgica et Materialia, Vol. 33 (1995) No. 8, pp. 1239-1244.

[6] Chernenko V.A., L'vov V.A., Cesari E., Pons J., Rudenko A.A. et al., "Stress-strain behaviour of Ni-Mn-Ga alloys: experiment and modelling ", Materials Science and Engineering A, Article in Press.

[7] du Plessis A, Jessiman A., Muller G., van Schoor M., "Latching valve control using ferromagnetic shape memory alloy actuators", Proc. of SPIE 2003, Vol. 4333 (August 2003) , pp. 320-331.

[8] Engdahl G., "Handbook of giant magnetostrictive materials", Academic Press, San Diego, 2000, p. 386.

[9] Ezer Y., Sozinov A., Kimmel G., Eteläniemi V., D'Anci A., et. al., "Magnetic shape memory (MSM) effect in textured pocrystalline Ni2MnGa", Proc. SPIE 1999, Vol. 3675 (July 1999) , pp. 244-251.

[10] Ferreira P.J., Vander Sande J.B., "Magnetic field effects on twin dislocations", Scripta Materialia, Vol. 41 (1999) No. 2, pp. 117-123.

[11] Funakubo H. (Ed.), "Shape memory alloys", Gordon and Breach, New York, 1986, p. 275.

[12] Heczko O. and Straka L., "Temperature dependence and temperature limits of magnetic shape memory effect", Journal of Applied Physics, Vol. 94 (2003) No. 11, pp. 7139-7143.

[13] Heczko O. and Ullakko K., "Effect of temperature on magnetic properties of Ni-

Mn-Ga magnetic shape memory (MSM) alloys", IEEE Trans. on Magnetics, Vol. 37 (2001) No. 4, pp. 2672-2674.

[14] Heczko O., Jurek K., Ullakko K., "Magnetic properties and domain structure of magnetic shape memory Ni-Mn-Ga alloy", Journal of Magnetism and Magnetic Materials, Vol. 226-230 (2001) , pp. 996-998.

[15] Heczko O., Sozinov A., Ullakko K., "Giant field-induced reversible strain in magnetic shape memory NiMnGa alloy", IEEE Trans. Magnetics, Vol. 36 (2000) No. 5, pp.3266-3268.

[16] Henry C.P., Feuchtwanger J., Bono D., Marioni M., Tello P.G. et al., "AC performance and modelling of ferrmomagnetic shape memory actuators", Proc. of SPIE 2001, Vol. 4333 (2001) , pp.151-162.

[17] Hirsinger L., Lexcelent C., "Modelling detwinning of martensite platelets under magnetic and stress actions on Ni-Mn-Ga alloys", Journal of Magnetism and Magnetic Materials, Vol. 254-255 (2003) , pp. 275-277.

[21] Jääskeläinen A., "Master Thesis, Magnetomechanical properties of Ni2MnGa", Helsinki University of Technology, Department of Material Science, 2001, p. 67.

[18] James R. D. and Wuttig M., "Magnetostriction of martensite", Philosophical Magazine A, Vol. 77 (1998) No. 5, pp. 1273-1299.

[19] Jeong S., Inoue K., Inoue S., Koterazawa K., Taya M., Inoue K., "Effect of magnetic field on martensite transformation in a polycrystalline Ni2MnGa", Materials Science & Engineering A, Article in Press.

[20] Jokinen T., Suorsa I., Ullakko K., "Magnetic Shape Memory Materials - New Actuator Materials for Electromechanical Devices", Proc. Speedam 2000 conference, 13-16 June 2000, Ischia, Italy, pp. B4-5 - B4-12.

[22] Kajaste J., Kauranne H., Suorsa I., Pietola M., "Magnetic shape memory (MSM) actuator as linear motor in proportional control valves", Proc. of IFK2004 conference, 25-26 March 2004, Dresden, Germany, .

[23] Kakeshita T., Takeuchi T., Fukuda T., Suburi T., Oshima R,Muto S.,Kishio K., "Magnetic field-induced martnsitic transformation and giant magnetostriction in Fe-Ni-Co-Ti and ordered Fe3Pt shape memory alloys", Material Transactions, JIM, Vol. (2000) No. 8, pp. 882-887.

[24] Karaca H.E. , Karaman I., Lagoudas D.C., MAier H.J., Chumlyakov Y.I., "Recoverable stress-induced martensitic transformation in a ferromagnetic CoNiAl

alloy", Scripta materialia, Vol. 49 (2003) No. 9, pp. 831-836.

[25] Kohl M., Brugger D., Ohtsuka M., Takagi T., "A novel actuation mechanism on basis of SMA thin films", Sensors and Actuators A, Article in Press.

[26] Kuhnen K., Janocha H., Schommer M., "Exploitation of inherent sensor effects in magnetostrictive actuators", Proc. of SPIE 2001, (July 2001) , pp. 367-370.

[27] L'vov V.A., Gomonaj E.V., Chernenko V.A., "A phenomenological model of ferromagnetic martensite", Journal of Physics: Condensed Matter, Vol.10 (1998) No. 21, pp. 4587-4596.

[28] Likhachev A.A, Sozinov A, Ullakko K, "Influence of external stress on reversibility of magnetic-field-controlled shape memory effect in Ni-Mn-Ga", Proc. of SPIE 2001, Vol. 4333 (2001) , pp.197-206.

[29] Likhachev A.A. and Ullakko K., "Magnetic-field-controlled twin boundary motion and giant magneto-mechanical effects in Ni-Mn-Ga Shape memory alloy", Physics Letters A, Vol. 275 (2000) No. 1-2, pp. 142-151.

[30] Likhachev A.A. and Ullakko K., "Quantitative Model of Large Magnetostrain Effect in Ferromagnetic Shape Memory Alloys", European Physical Journal B, 14 (2000) No. 263, pp. 263-267.

[31] Likhachev A.A. and Ullakko K., "The model development and experimental investigation of giant magneto-mechanical effects in Ni-Mn-Ga", Journal of Magnetism and Magnetic Materials, Vol. 226-230 (2001) , pp. 1541-1543.

[32] Likhachev A.A., Sozinov A., Ullakko K., "Different modelling consepts of magnetic shape memory and their comparison with some experimental results obtained in Ni-Mn-Ga", Material Science and Engineering A, Article in Press.

[33] Likhachev A.A., Sozinov A., Ullakko K., "Optimizing work output in Ni-Mn-Ga and other ferromagnetic shape-memory alloys ", Proc. of SPIE 2002, Vol. 4699 (July 2002) , pp. 553-563.

[34] Lundgren A., Tiberg H., Kvarnsjö L., Engdahl G., Bergqvist A., "A magnetostrictive electric generator", IEEE Trans. on Magnetics, Vol. 29 (1993) No. 6, pp. 3150.

[35] Madden J., "Properties of electroactive polymer actuators", Proc. of Actuator 2004 conference, 14-16 June 2004, Bremen, Germany, pp. 338-343.

[36] Marioni M.A, O'Handley R.C., Allen S.M., "Pulsed magnetic field-induced

actuation of Ni-Mn-Ga single crystals", Applied Physics Letters, Vol. 83 (2003) No. 19, pp. 3966-3968.

[37] Mogynyy G., Glavatskyy I., Glavatska N., Söderberg O., Ge Y., Lindroos V.K., "Crystal structure and twinning in martensite of Ni1.96Mn1.18Ga0.86 magnetic shape memory alloy", Scripta Materialia, Vol. 48 (2003) No. 10, pp. 1427-1432.

[40] Müllner P. and Ullakko K., "The of a magnetic/electric field on a twinning dislocation", Physical Status Solidi B, Vol. 208 (1998) No. 1, pp. R1-R2.

[41] Müllner P., Chernenko V.A., Kostorz G., "A microscopic approach to the magnetic-field-induced deformation of martensite (magnetoplastiticity)", Journal of Magnetism and Magnetic Materials, Vol. 267 (2003) No. 3, pp. 325-334.

[42] Müllner P., Chernenko V.A., Kostorz G., "Large cyclic magnetic-field-induced deformation in orthorombic (14M) Ni-Mn-Ga martensite", Journal of Applied Physics, Vol. 95 (2004) No. 3, pp.1531-1536.

[43] Müllner P., Chernenko V.A., Kostorz G., "Stress-induced twin rearrangement resulting in change of magnetization in a Ni-Mn-Ga ferromagnetic martensite", Scripta Materialia, Vol. 49 (2003) No. 2, pp. 129-133.

[44] Müllner P.,Chernenko V.A., Wollgarten M., Kostorz G., "Large cyclic deformation of a Ni-Mn-Ga shape memory alloy induced by magnetic fields", Journal of Applied Physics, Vol. 92 (2002) No. 11, pp. 6708-6713.

[38] Murray S.J., Marioni M., Allen S.M. and O'Handley R.C., "6% magnetic-field-induced strain by twin-boundary motion in ferromagnetic Ni-Mn-Ga", Applied Physics Letters, Vol. 77 (2000) No. 6, pp. 886-888.

[39] Murray S.J., O'Handley R.C., Allen S.M., "Model for discontinious actuation of ferromagnetic shape memory alloy", Journal of Applied Physics, Vol. 89 (2001) No. 2, pp. 1295-1301.

[45] O'Handley R.C., "Model for strain and magnetization in magnetic shape memory alloys", Journal of Applied Physics, Vol. 83 (1998) No. 6, pp. 3263-3270.

[46] O'Handley R.C., "Modern magnetic materials principles and applications", John Wiley & Sons, New York, USA, 2000, p. 740.

[47] Oikawa K., Ohmori T., Tanako Y., Morito H., Fujita A., Kainuma R. et al., "Magnetic and martensitic phase transitions in ferromagnetic Ni-Ga-Fe shape memory alloys", Applied Physics Letters, Vol. 81 (2002) No. 27, pp. 5201-5203.

[48] Pan Q. and James R.D., "Micromagnetic study of Ni2MnGa under applied field (invited)", Journal of Applied Physics, Vol. 87 (2000) No. 9, pp. 4702-4706.

[49] Pasquale M., "Mechanical sensors and actuators", Sensors and Actuators A, Vol. 106 (2003) No. 1-3, pp. 142-148.

[50] Pasquale M., Sasso C., Besseghini S., Passaretti F., Villa E., Sciacca A., "NiMnGa polycrystalline magnetically activated shape memory alloys", IEEE Trans. on Magnetics, Vol. 36 (2000) No. 5, pp.3263.

[51] Paul D.I., Marquiss J., Quattrotchi D., "Theory of magnetization: Twin boundary interaction in ferromagnetic shape memory alloys", Jounal of Applied Physics, Vol. 4699 (July 2002) No. 8, pp. 4561-4565.

[52] Pons J., Chernenko V.A., Santamarta R., Cesari E., "Crystal structure of martensite phases in Ni-Mn-Ga shape memory alloys", Acta Materialia, Vol. 48 (2000) No.12, pp. 3027-3038.

[53] Quandt E., Wuttig M., "Comparison of joule and twin induced magnetostriction", Proc. of Actuator 2004 conference, 14-16 June 2004, Bremen, Germany, pp. 359-362.

[54] Sakamoto T., Fukuda F., Kakeshita T., Takeuchi T., Kishio K., "Magnetic field-induced strain in iron-based ferromagnetic shape memory alloys", Journal of Applied Physics, Vol. 93 (2003) No. 10, pp. 8647-8649.

[55] Shield T.W., "Magnetomechanical testing machine for ferromagnetic shape-memory alloys", Review of Scientific Instruments, Vol. 74 (2003) No. 9, pp. 4077-4088.

[56] Shield T.W. and Cui J., "Magneto-mechanical behaviour of a ferromagnetic shape memory alloy Fe3Pd", Proc. SPIE 2002, Vol. 4699 (July 2002) , pp. 251-262.

[57] Sozinov A., Likhachev A.A. , Lanska N., Ullakko K., "Giant magnetic-field-induced strain in NiMnGa seven layered martensite phase", Applied Physics Letters, Vol. 80 (2002) , pp. 1746-1748.

[58] Sozinov A., Likhachev A.A., Lanska N,Söderberg O.,Ullakko K,Lindroos V.K., "Stress- and magnetic-field-induced variant rearrangement in Ni-Mn-Ga single crystal with seven-layered martensitic structure", Material science & Engineering, Article in Press.

[59] Sozinov A., Likhachev A.A., Ullakko K., "Crystal structures and magnetic anisotropy properties of Ni-Mn-Ga martensitic phases with giant magnetic-field-induced strain ", IEEE Trans. Magnetics, Vol. 38 (2002) No. 5, pp. 2814-2816.

[60] Sozinov A., Likhachev A.A., Ullakko K., "Magnetic and magnetomechanical properties of Ni-Mn-Ga alloys with easy axis and easy plane of magnetization", Proc. SPIE 2001, Vol. 4333 (July 2001) , pp.189-196.

[61] Straka L. and Heczko O., "Superelastic response of Ni-Mn-Ga martensite in magnetic fields and a simple model", IEEE Trans. on magnetics, Vol. 39 (2003) No. 5, pp. 3402-3404.

[62] Straka L., Hetzko O., Lanska N., "Magnetic properties of various martensitic phases in Ni-Mn-Ga alloy", IEEE Trans. on Magnetics, Vol.38 (2003) No. 5, pp. 2835-2837.

[63] Suorsa I., Pagounis E., Ullakko K., "Position dependent inductance based on magnetic shape memory materials", sent for review process to Sensors and Actuators A .

[64] Suorsa I., Tellinen J., Aaltio I., Ullakko K., "MSM-sensor", Patent FI 20030333, (Pending), 2003.

[65] Tellinen J., "A Simple Scalar Model for Magnetic Hysteresis", IEEE Trans. on Magnetics, Vol. 34 (1998) No. 4, pp. 2200-2206.

[66] Tellinen J., "Efficiency of MSM material, technical notes", Adaptamat Ltd., unpublished.

[67] Tellinen J., "Small power actuator, technical notes", Adaptamat Ltd., unpublished.

[68] Tellinen J., Suorsa I., Jääskeläinen A., Aaltio I., Ullakko K., "Basic Properties of Magnetic Shape Memory Actuators", Actuator 2002 confence, 12-14 June 2002, Bremen, Germany, 527-530.

[69] Tickle R., James R.D., "Magnetic and magnetomechanical properties of Ni2MnGa", Journal of Magnetism and Magnetic Materials, Vol. 195 (1999) No. 3, pp. 627-638.

[70] Tickle R., James R.D., Shield T., Wuttig M., Kokorin V.V., "Ferromagnetic shape memory in NiMnGa system", IEEE Trans. on Magnetics, Vol. 35 (1999) No. 35, pp. 4301-4310.

[71] Uchino K., "Piezoelectric actuators 2004 materials, design,drive/control, modelling and applications", Proc. of Actuator 2004 conference, 14-16 June 2004, Bremen, Germany, pp. 38-47.

[72] Ullakko K., "Magnetically controlled Shape Memory Alloys: A New Class of Actuator Materials", Journal of Material Engineering and Performance, Vol. 5 (1996) , 405-409.

[73] Ullakko K., EzerY., Sozinov A, Kimmel G, Yakovenko P., Lindroos V. K., "Magnetic-Field-Induced Strains in Polycrystalline Ni-Mn-Ga at room temperature", Scripta Materialia, Vol. 44 (2001) No. 3, pp. 475-480.

[74] Ullakko K., Huang J.K., Kokorin V.V. and O'Handley R.C., "Magnetically Controlled Shape Memory Effect in Ni2MnGa Intermetallics", Scripta Materialia, Vol. 36 (1997) No. 10, pp. 1133-1138.

[75] Wuttig M., Li M., Craciunescu C., "A new ferromagnetic shape memory alloy system", Scripta materialia, Vol. 44 (2001) No. 10, pp.2393-2397.

[76] Yamamoto Y., Eda H., Mori T., Rathore A., "Three-dimensional magnetostrictive vibration sensor: development, analysis and applications", Journal of Alloys and Compounds, Vol. 258 (1997) , pp. 107-113.

ISBN 951-22-7644-5
ISBN 951-22-7645-3 (PDF)
ISSN 1795-2239
ISSN 1795-4584 (PDF)